Development and fluctuation of crystal orientation fabric ~~and microstructures and deformational regimes~~ in the deep sections ~~and overall layered structures~~ of the Dome Fuji ice core, Antarctica: impacts of dust particles and migration recrystallization

Tomotaka Saruya[1], Atsushi Miyamoto[2], Shuji Fujita[1,3], Kumiko Goto-Azuma[1,3], Motohiro Hirabayashi[1], Akira Hori[4], Makoto Igarashi[1], Yoshinori Iizuka[5], Takao Kameda[4], Hiroshi Ohno[4], Wataru Shigeyama[3*], Shun Tsutaki[1,3]

[1] National Institute of Polar Research, Tokyo 190-8518, Japan
[2] Institute for the Advancement of Graduate Education, Hokkaido University, Sapporo 060-0817, Japan
[3] Polar Science Program, Graduate Institute for Advanced Studies, SOKENDAI, Tokyo 190-8518, Japan
[4] Kitami Institute of Technology, Kitami 090-8507, Japan
[5] Institute of Low Temperature Science, Hokkaido University, Sapporo 060-0819, Japan

[*]Currently at: JEOL Ltd., Tokyo, Japan

Correspondence: Tomotaka Saruya (saruya.tomotaka@nipr.ac.jp), Atsushi Miyamoto (miyamoto@high.hokudai.ac.jp), Shuji Fujita (sfujita@nipr.ac.jp)

Added (or partially modified)

Moved

Modified Figure

~~Removed~~

~~An in-depth examination of the rheology in the deep sections of polar ice sheets is crucial for understanding glacial flow.~~ This study ~~investigates~~ investigated the crystalline textural properties of ~~a 3035 meter long~~ an Antarctic deep ice core having a length of 3035 m acquired~~, drilled~~ at an inland plateau dome, with a focus on the depths below 2400 m ~~lowermost ~20%~~. ~~Inland plateau domes provide a unique opportunity to study ice deformation processes with minimal influence from simple shear. We analyze the~~ ~~The crystal orientation fabrics associated with of both the~~ *c*- ~~and~~ *a*-axes ~~were assessed and the data~~ The cluster strength ~~distribution and texture~~ of the *c*- ~~and~~ *a*-axes were ascertained, using~~, we employed three methods:~~ the dielectric tensor method to assess ~~determine~~ the ~~(DTM) for~~ bulk properties of thick sections~~,~~ and the detailed orientation of c- and a-axes were determined using the Laue X-ray diffraction technique ~~for detailed crystal grain orientations~~. Furthermore, *a*-axes distributions were determined by the Laue X-ray diffraction technique. The *c*- and *a*-axes fabric data were compared~~, comparing them~~ with various other characteristics of the same ice core ~~properties measured from the ice core~~. ~~To examine the, and an automatic ice fabric analyzer for grain by grain analysis using thin sections~~. ~~Microstructural observations were made using optical microscopy.~~ ~~DTM Dielectric tensor method provided preferred *c*-axis orientations as eigenvalues of the orientation tensor with high sampling frequency, spatial resolution, and continuity, offering statistical significance. Laue X-ray diffraction clarified detailed preferred orientations of both *c*- and *a*-axes., while the automatic fabric analyzer tracked *c*-axis orientation variations among individual grains. Microstructural images revealed dynamic recrystallization. In the uppermost ~80% thickness zone (UP80%),~~ The clustering strength of the single-pole *c*-axis fabric ~~steadily increased, reaching reached a maximum at the bottom~~ was at a maximum at depths between 2400 and 2640 m~~, driven primarily by vertical compression~~. ~~Below 1800 m in the UP80%,~~ The relationship between cluster strength and the concentration of dusty impurities was found to change at approximately ~~changed around~~ 2640 m and fluctuations in strength increased significantly below this depths. ~~Layers with varying concentrations of dusty impurities showed different rates of cluster strength evolution growth, a pattern that persisted until 2650 m. In the lowermost ~20% zone (LO20%), the *c*-axis clustering strength trend changed around 2650 m with substantial fluctuatios~~ Impurity-rich layers maintained a high degree of ~~stronger~~ clustering~~, while impurity poor~~

whereas layers having fewer impurities showed relaxation, ~~likely due to the emergence of new grains with *c*-axis orientations offset from the existing cluster and migration recrystallization. These impurity-poor~~ The latter layers also exhibited features of bulging and grain boundary migration. ~~migrating grain boundaries, with a decrease in grain aspect ratio~~. ~~Additionall In such ice,~~ In ice such as this, the degree of *a*-axis organization was increased with ~~progressed, displaying~~ one or two sets of three preferred orientations ~~within the *a*-axis girdle~~., ~~orthogonal to the *c*-axis cluster, possibly due to crystal twinning. These findings confirm that dislocation creep is the primary deformation mechanism in polar ice sheets. In the LO20%,~~ Dynamic recrystallization evidently played ~~plays~~ a critical role, with more pronounced effects in impurity-poor layers than in impurity-rich layers. ~~enabling the continuation of~~ This phenomenon promoted the relaxation of *c*-axis clustering deformation on dislocation-creep-based deformation and ~~forming~~ organization of the *a*-axis ~~organization within the *a*-axis girdle~~. Below 2580 m, the angles of inclination of the *c*-axes cluster and layers were significantly deviated from the vertical, suggesting the system rotated as a rigid body as a result of simple shear. ~~, particularly under at the higher temperatures closer to the bed. Additionally, we find that *c*-axis layers and~~ ~~The *c*-axis cluster axes were found to rotate meridionally due to as a result of rigid body rotation stemming from simple shear strain above the subglacial slopes. Insights The present insights into these nonlinear, irreversible processes offer vital clues for provide an improved understanding of the 3D three-dimensional structure of polar ice sheets. leading to inhomogeneous deformation, the formation of folds, faults, and mixing between layers at various thickness scales.~~

1. Introduction

~~1.1 Modeling ice sheets: challenges and insights from crystals to continents~~

~~The polar ice sheets are massive bodies of ice on Earth. With ongoing global warming, there is a deep concern about the trend of these ice sheets contributing to sea level rise (e.g., Church et al., 2013). Continuous improvement of reliable predictive models for this phenomenon is crucial. However, there are many key processes that govern the flow of ice sheets, making the modelling of these sheets complex. Although many essential processes exist, many are not included in modelling efforts due to insufficient understanding (e.g., Pattyn et al., 2008). Deciphering the dynamic layer structure within the ice sheet is one of the most critical challenges (e.g., Young et al., 2017).~~

~~1.2 Crystal anisotropy and ice sheet dynamics~~

Crystal orientation fabric is one of the most important factors controlling the physical properties of polar ice sheets. In particular, both the deformation and flow of ice sheets are significantly affected by the crystal orientation fabric and the deformation ~~The~~ response of individual ice crystals to stress exhibits a pronounced anisotropy ~~in deformation~~. Specifically, these crystals ~~Crystals~~ readily undergo shearing along the slip systems within their basal planes, ~~whereas shearing on alternate slip systems is significantly more difficult, nearly a hundredfold~~ whereas nearly a hundred times greater (shear) stress must be applied to induce deformation along other slip systems within the crystals (e.g., Duval et al., 1983). In the case that ice are randomly oriented, these crystals will behave isotropically while nonrandom orientations will result in anisotropic behavior. ~~The overall rate of deformation in a polycrystalline aggregate under stress is influenced by the orientation of its constituent crystals. If crystals within an aggregate are randomly oriented, the material will behave isotropically; however, if the orientations of the crystals are not random, the material will show anisotropic behavior. The study of anisotropic ice deformation has been conducted historically. They were done through theoretical research (e.g., Alley, 1992; Azuma, 1995; Azuma and Goto-Azuma, 1996; Castelnau et al., 1996; Gödert and Hutter, 1998; Johnson, 1977), and through laboratory experiments (e.g., Duval, 1981; Duval and Le Gac, 1982; Shoji and Langway Jr., 1985; Pimienta et al., 1988; Budd and Jacka, 1989; Castelnau et al., 1998; Goldsby and Kohlstedt, 2001; Qi et al., 2019; Fan et al., 2020). These laboratory based studies are characterized by experimental setting of strain rate by more than several orders of magnitude, and under temperature close to melting point, typically between -20 and 0 °C. Therefore, these laboratory-based knowledge can be a valuable reference mainly for such conditions. To better understand rheology of polar ice sheets, analyses of ice texture sampled from polar ice sheets play another essential role. Examples of Antaretic deep ice core include, Dome Fuji (hereinafter, DF) ice core (e.g., Azuma et al., 2000 and Saruya et al., 2022b), EPICA Dome C (hereinafter, EDC) ice core (e.g., Wang et al., 2003, Durand et al., 2007, 2009), Byrd ice core (Gow and Williamson, 1976) , EDML ice core (e.g., Weikusat et al., 2017), Mizuho Station ice core (Fujita et al., 1987; Higashi et al., 1988), Talos Dome ice core (Montagnat et al., 2012), WAIS Divide ice core (Fitzpatrick et al., 2014) and South Pole (SPICE) ice core (Abbasi et al., 2024). Examples of Greenland ice sheet include GRIP ice core (Thorsteinsson et al., 1997), NEEM ice core (Montagnat et al., 2014), EGRIP ice core (Stoll et al., 2021a, 2022; Richards et al., 2023) and among others. In these studies, the influence of anisotropy on the movement of ice aggregates is so substantial that comprehending its impact on the expansive flow patterns of ice sheets is essential (e.g., Castelnau et al., 1998; Mangeney et al., 1997; Paterson, 1991; Russell Head and Budd, 1979; Thorsteinsson et al., 1999). For instance, during the internal deformation of the ice sheet, the flow forms preferred orientations of crystal axes, at the same time, the ice flow is modulated based on them.~~ As an example, the internal deformation of an ice sheet can lead to the preferred orientations of ice crystals that, in turn, affects the flow of the ice sheet. The ice flow is also affected ~~modulated~~ by the concentrations of ionic species and dust particles, as well as by disturbances or folds in the layer structure (e.g., Cuffey and Paterson, 2010, Durand et al., 2007, Saruya et al., 2022b). These factors can introduce either positive or negative feedback that modulates ~~modulating the~~

flow characteristics of the ice sheet. Considering this complexity, it is evident that ~~complex nature of ice, we need a~~ systematic understanding of the ~~layered~~ internal layered structure of polar ice sheets is required. ~~over space and time~~. ~~An important method for understanding these is to conduct analysis of ice cores in terms of ice dynamics, which provides a "ground truth" perspective of the ice.~~

~~1.3 Advantages of ice cores from dome regions in central plateau area of the ice sheets~~

~~The ice in the dome summit regions of central plateau areas on ice sheets offers an opportunity for studying ice deformation processes. In these regions, conditions are relatively simplified because it can be presumed that they are least affected by simple shear deformation. This deformation is typically caused by surface slope and gravity. Because of this simplicity, dome regions in central area of the ice sheets are often chosen as ice core drilling sites for the purpose of exploring the history of past climate changes. At the same time, these sites are ideal for investigating how processes related to deformational progress (such as dislocation creep and recrystallization) develop in a relatively simplified stress-strain environment and under moderate temperature gradients. Among the drilling sites in Antarctica shown in Figure 1, we can presume that so far only DF and EDC sites meet this condition. In fact, in the case of inland domes, ice deforms mainly by compression along the vertical. This is confirmed by the preferred orientation of *c* axes measured along cores drilled at these sites (as in references listed above), which exhibit a single pole distribution of the *c* axes. Similarly, this has been confirmed in the Greenland ice sheet with the GRIP core (Thorsteinsson et al., 1997). We note that there are also local domes at the edge of the ice sheet plateau, for example, Talos Dome (Urbini et al., 2008). Such a dome is characterized by lower elevation (of 2318 m), location facing to the coast, with annual accumulation rate much larger than those of central plateau (by 3–4 times), and migration at least in the last few centuries. Such a dome has higher instability, and it is suitable to investigate impact of more shear in contrast to the domes in the central plateau area. Evolution of preferred orientation of *c*-axes for the Talos Dome core was presented by Montagnat et al. (2012).~~

~~1.4 Exploring deep ice rheology and crystal properties~~

~~In ice sheets, the~~ The rheology in the deepest ~~deep ice (deepmost~~ several hundred meters~~)~~ of an ice sheet is complicated by geothermal effects and increased stresses resulting from the bedrock topography. ~~So far,~~ Even so, to date, there have been limited reports concerning on the crystal properties of ice near the bed at ~~dome summits of~~ central plateau dome summits of the ice sheets (e.g., Thorsteinsson et al., 1997; Durand et al., 2009, Faria et al., 2014a, Ohno et al., 2016). ~~The DF ice core was drilled on the Antarctic plateau (Figure 1). This location is at 77°19′ S latitude and 39°42′ E longitude, and 3,810 m above sea level. Annual surface mass balance (SMB) has ranged from approximately 24 to 28 kg m^{-2} y^{-1} over the last 5000 years (Oyabu et al., 2023), and the annual mean surface air temperature is −54.4°C (Yamanouchi et al., 2003). For the DF ice core, Ohno et al. (2016) revealed the air hydrates and water isotope composition of the deepest 1% thickness (3000–3035 m). These properties were found to retain the basic layered structure of ice core signals except in the deepest few meters. However, the investigation did not include the crystalline textural properties. For the EDC core (Figure 1), Durand et al. (2009) investigated the *c*-axis orientations of ice down to the very deep parts, using thin sections of ice (40 × 110 mm in width and 0.4 mm in thickness) sampled at every 11 m depth.~~ Deep ice is characterized by higher temperatures at~~, under~~ which enhanced phenomena related to ~~enhancement of~~ molecular ~~transport phenomena is an issue~~ becomes important (e.g., Petrenko and Whitworth, 1999). ~~The molecular transport~~ These phenomena include plastic deformation, the molecular diffusion processes and recrystallization, and studies concerning dynamic recrystallization in ice sheets have been performed (e.g., Poirier 1985; De La Chapelle et al. 1998; Humphreys and Haterly 2004; Weikusat et al. 2009; Kipfstuhl et al. 2009; Montagnat et al. 2012, 2014; Faria et al., 2014a and Stoll et al., 2021a). The work reported herein took advantage of the unique opportunity that the Dome Fuji (DF) ice core offers with regard to assessing the role of dynamic recrystallization in the formation of textures and fabrics in the deeper

parts of the East Antarctic ice sheet. ~~Dynamic recrystallization within ice sheet has been widely investigated historically, as reviewed in papers or textbooks (e.g., Poirier 1985; Humphreys and Haterly 2004; Faria et al., 2014a, b) or individual papers (e.g., De La Chapelle et al. 1998; Weikusat et al. 2009, Kipfstuhl et al. 2009, Montagnat et al. 2012, 2014; Stoll et al., 2021a). Exploring deep ice rheology and crystal properties, dynamic recrystallization is one of main focuses in this paper.~~

~~1.5 Advancing ice sheet dynamics: The development and role of crystal orientation fabric~~

The crystal orientation fabric contains information concerning the history of deformation ~~of deformational history~~, grain growth and recrystallization (e.g., Cuffey and Paterson, 2010; Faria et al., 2014a, b). Saruya et al. (2022b) investigated the ~~layer structures~~ development of the *c*-axis fabric in the DF ice core at depths above 2400 m ~~uppermost (shallower) ~80% thickness zone (hereinafter, UP80%) of the DF ice core. They used~~ using thick sections of ice (ranging in thickness from 33 to 79 mm) ~~employing~~ in conjunction with the principle of the radio-wave birefringence ~~to obtain information from a volume much larger than that of thin sections of ice in typical thickness of about 0.3–0.5 mm. The sampling volumes between the two methods (thick-section method and thin-section method) differ by around two orders of magnitude.~~ Using the dielectric tensor method (hereinafter, DTM), this prior work assessed the degree of ~~they continuously measured~~ dielectric anisotropy (~~denoted as~~ $\Delta\varepsilon$) along the ice cores ~~with high resolution, involving ice volumes of cylinders measuring 16–38 mm in effective radio beam diameter and 33–79 mm in radio propagation thickness.~~ This ~~$\Delta\varepsilon$~~ parameter is defined as the difference in relative permittivity along the vertical (~~denoted as~~ ε_v) and in the horizontal planes (~~denoted as~~ ε_h)~~. Thus~~, such that $\Delta\varepsilon = \varepsilon_v - \varepsilon_h$~~. $\Delta\varepsilon$ is an indicator of~~ and indicates the clustering strength of the *c*-axes. The value of $\Delta\varepsilon$ is linearly compatible with the normalized eigenvalues of the second order tensor (Saruya et al., 2022a, b). ~~The normalized eigenvalues are often used to express the degree of the *c*-axes clustering. Thus, continuous profiling with DTM is an innovative and powerful tool to directly measure the normalized eigenvalues for preferred orientation of *c*-axes with symmetry (such as single pole, girdle type or superposition of them).~~ These authors also found that $\Delta\varepsilon$ steadily increases with depth~~, showing~~ but also exhibits fluctuations ~~in the UP80%~~. In addition, significant decreases in $\Delta\varepsilon$ were ~~found~~ identified at depths ~~of~~ associated with major glacial-to-interglacial transitions. These observed changes in $\Delta\varepsilon$ ~~are~~ can be explained ~~as~~ by variations in the deformational history of regions of the ice sheet over which vertical compression is the primary cause of stress. ~~variations in the deformational history of the vertical compression. Moreover, fluctuations in $\Delta\varepsilon$ along neighboring depths were enhanced during the glacial/interglacial transitions. Furthermore, the~~ The $\Delta\varepsilon$ data have additionally been shown to positively correlate ~~exhibited a positive correlation~~ with the concentration of chloride ions in the ice and ~~an inverse correlation~~ inversely correlated with the amount of dust particles. Since ~~these factors~~ both chloride ions and dust originate from atmospheric deposition, Saruya et al. (2022b) proposed that the fluctuations in the clustering strength might be common across wide areas of ice sheets. ~~This hypothesis for the Dome Fuji core, in part, differs from an existing hypothesis for the EDC ice core given by Durand et al. (2007). That is, the changes in the clustering strength (which increase sharply with depth) were associated with positive feedback between variations in ice viscosity and the impact of a shear stress component, also increasing with depth (Durand et al., 2007). A basic difference is that Saruya's hypothesis did not need to assume the presence of shear deformation as a prerequisite to explain the observed fluctuations of the clustering strength whereas Durand et al. (2007) suggested the impact of shear and the positive feedback was important.~~

On this basis, the present research studied the deepest 20% of the DF core (specifically, the depth range of 2400–3035 m) to provide a more complete understanding of the development of the texture and fabric throughout the entire ice sheet column. ~~Following this previous study, research focusing on the lowermost (deepest) approximately 20% thickness zone (ranging from about 2400 m to the deepest ice at 3035 m) remains to be done, to examine textural data for the entire thickness of the ice sheet. Hereinafter, we refer to this zone as LO20%.~~ A major ~~difficulty~~ challenge to this work was the inclination of the ice sheet layers, which ~~became~~ becomes steeper at deeper depths (Dome Fuji Ice Core Project Members ~~hereinafter referred to as~~ (DFICPM), 2017). ~~In the present study, we extend the investigation to the LO20%. To investigate this, we~~ This research

utilized the DTM in conjunction with thick sections together with techniques utilizing thin sections, including ~~thick section-based method of (i) DTM, and thin section based methods such as (ii)~~ the Laue X-ray diffraction method and ~~(iii) the~~ microstructural observations. ~~We compare~~ The textural data obtained with these methods is compared herein with various datasets produced from prior studies of the same ice core. ~~We compare textural data by these methods with various data analyzed from the ice core.~~ This paper provides an advanced, ~~and most~~ updated dataset concerning ~~of~~ the crystal orientation fabric with regard to ~~for~~ both *c*-axis and *a*-axis along with additional ~~and other~~ textural data ~~for the entire thickness~~ of the DF ice core. ~~ice sheet at DF. We then discuss~~ Using these data, the development of the crystal orientation fabric as well as variations in the microstructure, layered structure and rheology of polar ice sheets is discussed~~, addressing differences in the existing hypotheses~~. ~~Our~~ This new ~~data will provide important clues for~~ information increases our understanding of the development of the layered structures ~~of~~ in ice sheets,~~ which leads to inhomogeneous deformation of layers across various layer thickness scales~~.

~~Furthermore, retrieving continuous ice core records covering snow deposition over more than 1 million years that correspond to ages of more than 1 million years presents a significant challenge in palaeoclimatology (e.g., Wolff et al., 2022). International Partnerships in Ice Core Sciences (IPICS) identified the retrieval of multiple ice cores that extends to 1.5 million years (symbolically named as the "oldest ice cores") as one of the most important challenges for ice core studies. Identifying suitable sites for drilling of such ice will require improved knowledge of the physical properties and the deformation history in different regions of the East Antarctic ice sheet. knowledge of englacial layers under various ice conditions.~~

2. DF ice cores

The DF ice core was drilled on the Antarctic plateau (Figure 1) at a location with 77°19' S latitude and 39°42' E longitude that was 3810 m above sea level. The ice thickness is 3028 ± 15 m (DFICPM, 2017).The annual surface mass balance at this location has ranged from approximately 24 to 28 kg m^{-2} y^{-1} over the last 5000 years (Oyabu et al., 2023) and the annual mean surface air temperature is –54.4°C (Yamanouchi et al., 2003). ~~At DF, deep~~ Deep ice cores have been drilled ~~twice~~ at DF on two occasions (e.g., Motoyama et al., 2020). The first core, DF1, ~~measuring~~ was 2503 m in length~~,~~ and was drilled in the 1990s. The second, DF2, had a 3035 m ~~long core,~~ and was drilled between 2004 and 2007 in a borehole 44 m away from the previous borehole (Figure 1c). ~~We used the~~ The DF2 core specimen was employed in the present study. ~~The~~ Both drilling sites are situated above a subglacial slope, positioned between bedrock high in the east and a subglacial trough with an ice thickness of ~~about~~approximately 3100 m in the west (Figures 1b and 1c). An ice thickness of ~~about~~ approximately 2850 m marks the boundary between a thawed bed (in the case of thicker ice) and a frozen bed (in thinner ice) (Fujita et al., 2012). It is ~~speculated~~ thought that spatially inhomogeneous basal melting has ~~caused~~ produced the ~~layer~~ localized inclination of layers ~~in localized areas~~ within the ice sheet (DFICPM, 2017). The layered structures ~~incline~~ are inclined by less than ~~about~~ approximately 5° ~~in~~ at the shallow depths ~~UP80% while~~ whereas in the deeper sections, ~~lower 20% (LO20%)~~, the inclination reaches ~~values up to~~ angles as high as 45° at a depth of 3000 m. Ohno et al. (2016) reported the distribution of air hydrates and isotopic composition of water in the deepest 1% (3000–3035 m) of the DF ice core. These factors were found to reflect the basic layered structure of ice core signals except in the deepest few meters. However, this prior work did not investigate the crystalline textural properties.

At present, DF is very close (within 10 km) to the dome summit and associated with a steep north-south surface mass balance gradient (Fujita et al., 2011; Tsutaki et al., 2022). This morphology impllies that the DF summit has migrated along this gradient in the north-south direction during glacial and interglacial periods over which the accumulation rate changed dramatically (e.g., Parrenin et al., 2016). Thus, DF is subject to deviatoric stress in the direction of maximum inclination at each time. ~~In terms of the *c*-axis fabric,~~ Azuma et al. (1999, 2000) reported that, in the case of the ~~at~~ DF1 core the *c*-axis fabric exhibited ~~the~~ an elongated single pole fabric that was ~~as the dome undergoes deviatoric strain depending on orientations~~. ~~This elongated single pole fabric is~~ already observable at shallow depths. In addition, Fujita et al. (2006) ~~discussed, based on~~

investigated DF using polarimetric radar sounding ~~at Dome Fuji, the amount of~~ and assessed the extent of radio wave birefringence caused by this elongated single pole fabric~~, up~~ to depths of ~~about~~ approximately 2200 m. ~~They~~ Fujita's work demonstrated that the orientations of the elongated single pole fabric were~~,~~ ~~are consistent~~ at least to this depth. Figure 1c ~~shows~~ present the ~~inferred~~ two principal axes assumed for ~~of~~ the elongated *c*-axis fabric as red cross, aligning with the orientation of the subglacial slope (WNW) and its orthogonal direction.

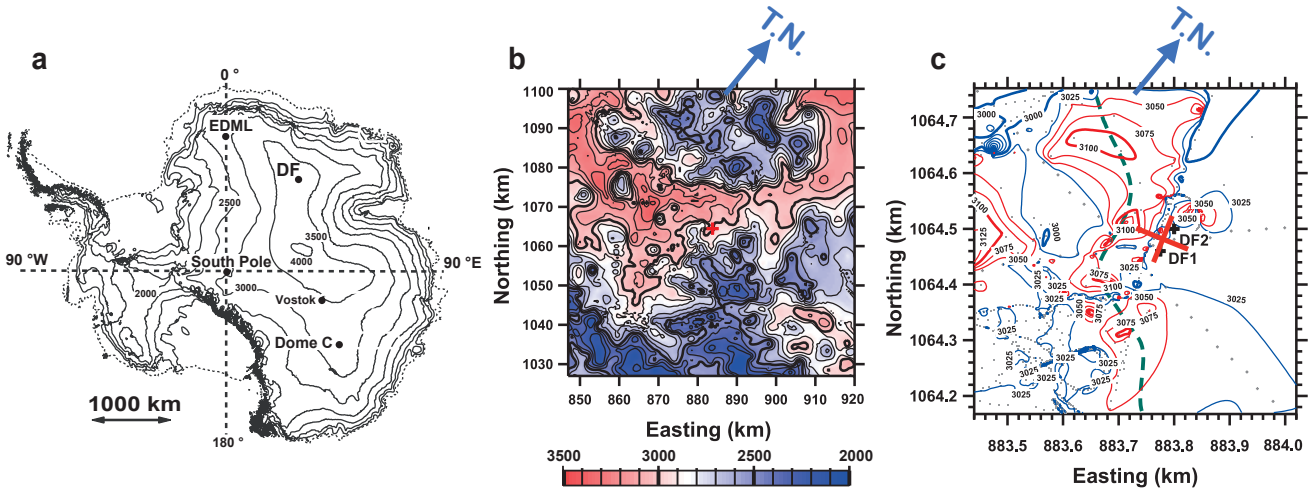

Figure 1. Maps of the coring Site. (a) Surface elevation a digital elevation model (~~DEM by~~ Bamber et al., 2009). Maps showing ice thickness over areas of (b) ~~and (c) show the thickness of the ice in areas of~~ 72 km^2 and (c) ~~square, and~~ 580 m^2 ~~square, respectively~~. ~~Marker~~ In (b) and (c) the ~~symbols~~ small red/black crosses near the ~~center~~ centre of each map indicate the coring site. T.N.~~stands~~ for indicates true north. In (c) ~~data points for~~ ice thickness ~~are represented~~ is indicated by dots ~~for the~~ representing data from Tsutaki et al. (2022) and by markers ~~for the~~ representing data from Eisen et al. (2020). Thin and thick areas are shown in red and blue respectively, and the boundary is set at a thickness of 3000 m. ~~A green bold~~ The bold green dashed line indicates the presence of the local trough. The DF coring sites ~~are~~ were located at the bank of this local trough, aligning with the estimated drainage routes of subglacial water (as shown in Figure 8d in Tsutaki et al., 2022). ~~On the Figure 1c,~~ In (c), two principal axes of the elongated single pole fabric inferred from the polarimetric radar sounding (Fujita et al., 2006) ~~is~~ are indicated as a large red cross.

3. Methods and samples

~~We~~ As noted, this work utilized the DTM based on thick sections together with ~~the thick-section-based method of DTM, as well as the thin-section-based methods of~~ the Laue X-ray diffraction method and the microstructural observation using thin sections. ~~On one hand, using DTM,~~ The DTM provided data concerning the *c*-axis fabric ~~data are provided as~~ in the form of eigenvalues with high sampling frequency, high spatial resolution, and continuity~~, thereby offering statistical significance~~. However, this method does not produce ~~data for~~ information regarding the crystal axes of individual grains. Additionally, if a cluster of *c*-axes is significantly inclined from the vertical, it is impossible to derive correct eigenvalues without knowing both the angle of inclination ~~angle of the *c*-axis cluster~~ and the horizontal orientation of the *c*-axis cluster. ~~On the other hand,~~ In contrast, the Laue X-ray diffraction ~~method allows us to clarify~~ technique provides detailed information ~~about~~ concerning both the *c*-axis and the *a*-axis of each crystal grain. Additionally, the use of an automatic fabric analyser (model G50, Russel–Head Instruments) allowed an assessment of variations in ~~is a very useful method for demonstrating how~~ crystal orientation ~~differs from one grain to another~~ between grains. Using both the G50 analyser and microscopy, ~~we conducted~~ microstructural observations were performed as a means of assessing ~~to investigate the signals of~~ dynamic recrystallization and grain morphology. The ~~judicious use of these~~ methods described above provided a significant quantity of data concerning variations in ~~provides unprecedentedly rich information on~~ crystalline texture along ice cores.

3.1 Dielectric Tensor Method

3.1.1 Method

The principles of the open resonator method for determining the relative permittivity (ε) of thin samples have been described in the literature (Jones, 1976a, b; Cullen, 1983; Komiyama et al., 1991). ~~We have~~ The authors have since developed this technique to allow investigation of ~~into a method for measuring the~~ tensorial permittivity of thick samples ~~by using~~ based on continuous radio birefringence ~~continuously~~ scanning along an ice core (Matsuoka et al., 1998; Fujita et al., 2009, 2014, 2016; Saruya et al., 2022a, b; Inoue et al., 2024). ~~We apply~~ The present work employed a microwave beam to study thick samples and~~. The~~ ε values were obtained as ~~are~~ volume-weighted averages within the volume encompassed by the Gaussian distribution of the beam. By setting the angle between the axis of the *c*-axis cluster and that of the electric field to approximately 45°, radio birefringence ~~occurs~~ was generated as a result of the ~~due to~~ macroscopic permittivity of the crystals (e.g., Hargreaves 1978). ~~When we sweep~~ Sweeping the radio wave frequency ~~frequencies~~ to detect resonances satisfying $TEM_{0,0,q}$ modes (where TEM ~~stands~~ is acronym for transverse electromagnetic and q is an integer) allowed ~~we detect~~ twin resonant peaks caused by the ~~two~~ dual permittivity components to be detected. These two components corresponded to ε along the axis of the *c*-axis cluster and ~~its~~ along the orthogonal axis, representing components on the plane of the electric field vector (orthogonal to the axis of beam incidence).

3.1.2 ~~The open~~ Open resonators and samples

~~We utilized an open resonator, employing frequencies between 26.5 and 40 GHz (No.1 in Table A1) for the ice in the LO20%. This resonator is different from the resonator used for the ice in the UP80%, employing frequencies between 15 and 20 GHz (No.2 in Table A1). Specifications of the two resonators are summarized in Table A1 in Supplementary Information A1.~~ This work employed two resonators (designated Nos. 1 and 2), the specifications of which are summarized in Table S1 in Supplementary Information Section 1. An open resonator employing frequencies between 26.5 and 40 GHz (entry 1 in Table S1) was utilized to assess the ice in the lowermost 20%. This resonator differed from that employed to study the ice above 2400 m, which operated at frequencies between 15 and 20 GHz (entry 2 in Table S1). ~~The~~ These two resonators, each having a semi-confocal shape with a flat mirror and a concave mirror, ~~are~~ were designed to produce beam diameters of 16 mm and 38 mm, respectively. The consistency of the data obtained with the two resonators was confirmed by comparing the $\Delta\varepsilon$ values at depths between 2400 and 2500 m (Figure S1 in Supplementary Information Section 1). The smaller beam size ~~means that the~~ of resonator No.1 allowed the analysis of ~~resonator is available for~~ smaller sized samples (~~for example,~~ such as narrow quadrangular prisms ~~samples~~) ~~and for~~ with higher spatial resolution ~~measurements~~. The No.1 and the No.2 resonators were able to analyze ~~can measure~~ ice specimens having thicknesses of ~~thickness~~ at least 40 mm and 90 mm, respectively. ~~Sizes~~ The sizes of the samples examined in this work are summarized ~~are given~~ in Figure 2 and Table S2. Both the upper and lower surfaces of each specimen were microtomed to ~~make very~~ provide extremely smooth and precisely parallel surfaces. The ~~sampling rate for the DTM involves continuous 20 mm step measurements along a 0.5-m-long core segment from every 2.5-m depth interval.~~ The DTM involved a series of measurements at 20 mm intervals along core segments having lengths of 0.5 m acquired at 2.5 m depth intervals. ~~For~~ In the case of samples acquired below ~~deeper than~~ 2736 m, ~~we rotated~~ the core axis was rotated horizontally in the open resonator apparatus ~~setup to achieve detectable~~ to ensure that the twin resonances could be detected. The experimental data were acquired at temperatures ~~were~~ in ~~a~~ the range of –30 ± 1.5 °C.

~~Along with the increased layer inclination,~~ In addition to increases in the layer inclination, the axis of the *c*-axes cluster also exhibited an increased inclination such that this axis deviated from~~, deviating~~ from the vertical (hereinafter, referred to as the angle of inclination angle) in the same direction ~~of the maximum layer slope~~ as the normal to the maximum layer slope. ~~We confirmed that these two are in the same vertical plane throughout the LO20%.~~ The relative orientation between each layer and the *c*-axes cluster was assessed by investigating the angle of inclination of the layer near the thin-sections used for the Laue X-ray diffraction method. These data confirmed that the horizontal direction for the *c*-axis cluster and the normal axis of

each layer were within the approximately same vertical plane throughout the lowermost 20% of the DF ice core. Additionally, the horizontal orientation of the *c*-axes cluster varied with depth due to the rotation of the ice cores. ~~Under conditions where~~ In the case that both the angle of inclination angle and horizontal orientation of the *c*-axes cluster ~~change~~ varied with depth, ~~we measure~~ only the non-principal components of the permittivity tensor were determined within the ice using the DTM. Since the electromagnetic wave used in the DTM method has a transverse electric field, if the surface of the actual plate-shaped sample does not align with the principal axes of the crystal tensor, only the components in the misaligned orientation will be obtained. This misaligned orientation is referred as non-principal. ~~To apply geometrical corrections~~ Geometrical corrections to translate from the measured non-principal components to the principal components were applied using both the angle of~~,~~ ~~we utilized information of both~~ inclination angle and horizontal orientation of the *c*-axes cluster as derived from *c*-axis fabric data ~~measured~~ acquired using a thin-section method. The procedures ~~for~~ used to perform these corrections are detailed in Supplementary Information Section 2. The non-principal components of the dielectric anisotropy ($\Delta\varepsilon'$) were also adjusted to align with the principal components ($\Delta\varepsilon$). ~~We also note~~ It should also be noted that the DTM is ~~also~~ a useful means of finding the to detect $\Delta\varepsilon$ values of ~~in~~ the girdle type ice fabrics. We can refer to the basic principles summarized in Supplementary Information Section 2~~, as girdle distribution of *a* axes in the figure~~.

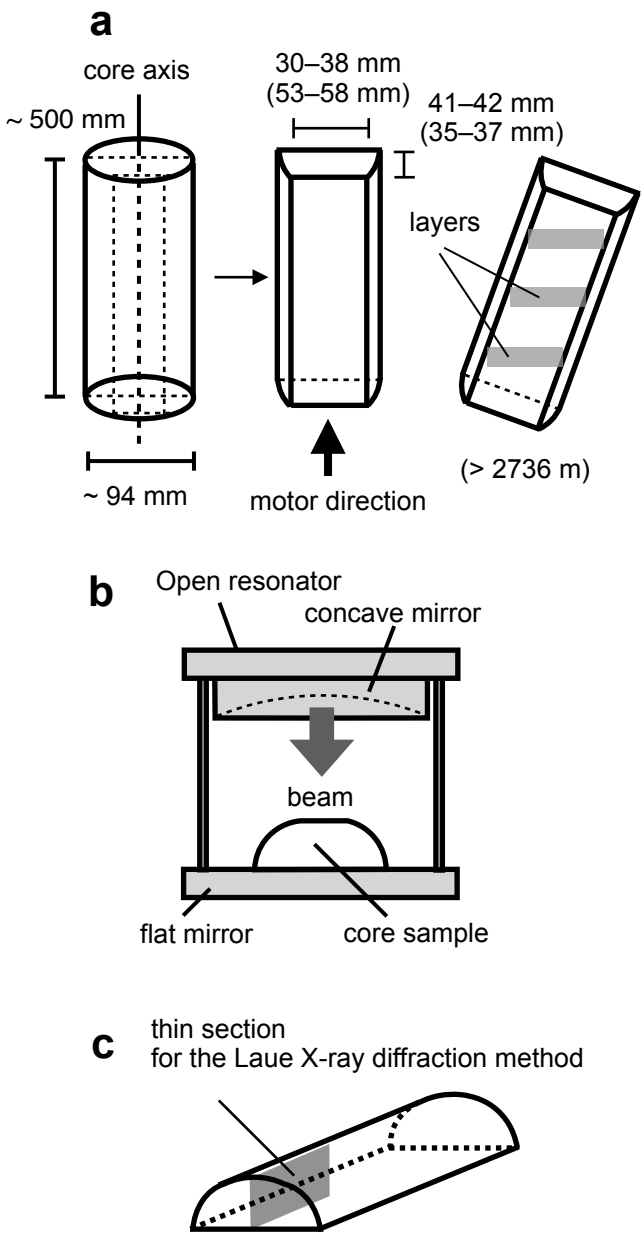

Figure 2. Diagrams of the (a) core cutting geometry and scanning direction, (b) the analytical setup as viewed from the front, and (c) the location of a thin section assessed using for the Laue X-ray diffraction method.

3.2 Characterizations by Laue X-ray diffraction method, microstructural observations and automatic fabric analyser

The Laue X-ray diffraction method was applied to thin sections measuring 100 × 45 mm (in the vertical and horizontal direction, respectively), and with thicknesses of less than 0.5 mm. This ~~method~~ technique can determine the orientations of all axes of each crystal grain with an accuracy on the order ~~of~~ 0.5 degree (Miyamoto et al., 2011). A total of 42 depths within the thickness of the lowermost 20% were selected for analysis and the Lauer Patterns were analysed after ~~After~~ obtaining all the Laue figures, the Laue patterns were analyzed. ~~In each thin section,~~ Here, the data for each thin section are expressed ~~we express the data~~ as the distribution of *c*-axes and *a*-axes on ~~the~~ a Schmidt net diagram. ~~In addition, we calculated the~~ The median inclinations of the *c*-axes with ~~reference~~ respect to the axis of the *c*-axes cluster were also calculated. The median inclination ~~is~~ was defined as ~~a~~ one half of the apex angle of the cone in which a one half of the measured *c*-axes ~~are~~ were included from the centre axis of the *c*-axes cluster.

Additionally, ~~we conducted~~ microstructure observations were carried out using both the G50 instrument and optical microscopy to investigate the manner in which ~~how~~ microstructural evolution affected the development of ~~affect~~ the *c*-axis fabric development and to assess fluctuations in ~~fluctuation on~~ the same thin section. These ~~measurements~~ analyses were performed at several preselected depths. ~~We prepared thin~~ Thin sections were prepared from the vertical plane of the ice cores, measuring 90 mm in the depth direction and 50 mm in the horizontal direction and with thickness of 0.5 mm ~~in thickness~~. ~~In addition, images of~~ Images of the *c*-axis fabric were obtained using the G50 automatic fabric analyser to investigate the relationship between ~~grain~~ the morphology and *c*-axis orientation of each grain. ~~Grain~~ The grain numbers included in a the Gaussian beam or in a thin section are ~~listed~~ provided in Table S3. ~~Depending on number of crystal grains in a beam or thin section, statistical significance is different. In some cases, moving averaging along the core is useful to gain more significance.~~

3.3 Grain size and layer inclination measurements

The grain sizes ~~were measured~~ at the DF site were ascertained in this work based on visual observations of faint differences ~~Operators from the ice processing team observed the crystal grains by noting a faint difference~~ in light reflectivity between grains and visible grain boundaries. While freshly cut surfaces did not exhibit ~~such~~ these features, the ice cores in storage developed these reflectivity variations ~~them~~ over time ~~due to the progress of~~ as sublimation progressed. ~~To measure the~~ The average surface area of each grain was determined using~~, we used~~ three circular gauges with diameters of 10, 20, and 40 mm and by counting the~~ The~~ number of grains on the core surface within the circle of the gauge was counted. The number of crystal grains within each circle typically ranged from several to 20mm, with an~~. The~~ estimated error was ~~up to~~ as high as 20% of the crystal quantity. These examinations were ~~This measurement was~~ performed ~~every~~ at 1.5 m intervals to a depth of 2967.5 m. Below this depth, ~~because of very large crystals,~~ the crystals were much larger and it became ~~it was~~ difficult to define the grain size. Changes in the angles ~~Additionally, we visually investigated the evolution growth~~ of the inclination ~~angle of the~~ of visible features ~~layers~~ (such as cloudy bands or tephra layers) relative to ~~from the horizon~~ horizontal were also investigated using a protractor. This process is explained in detail of the method is given in Supplementary Information section 1.3. ~~In this process,~~ It should be also be noted that this method did not take into account core rotation resulting from core breaks ~~was not considered~~. The present work provides detailed data supplementing that in a preliminary report (DFICPM, 2017). ~~In addition to our preliminary report on this point (DFICPM, 2017), this study provides detailed data.~~

4. Results

4.1 Depth-dependent variations in measured $\Delta\varepsilon'$, corrected $\Delta\varepsilon$ and ~~SD~~ standard deviation values

~~Results on~~ The $\Delta\varepsilon'$ data are presented in Figure 3~~. Examples of~~ while examples showing the continuous variation of $\Delta\varepsilon'$ along a ~~0.5 m~~ core segment having a length of 0.5 m are provided in Supplementary Information Section 3. Here, ~~Markers~~ the

symbols and error bars indicate the ~~average~~ mean values and the standard deviations (SDs) determined at 0.5-m intervals along the core sample~~. Dots~~ while dots represent raw data. Black and red symbols ~~represent~~ indicate data obtained without and with inclined measurements, respectively. Data ~~from both cases (~~ acquired without and with the horizontal samples ~~inclinations~~ inclined within the resonator~~)~~ are in agreement ~~at overlapping depths~~ over the depth range of 2630–2730 m~~, confirming the experimental principle~~ for which both measurements were performed. This outcome confirms that the horizontal rotation of the samples in the open resonator ~~give no influence on the measurement of the~~ did not affect the experimental relative permittivity values. ~~We note~~ Note that, ~~in the LO20%~~ overall, the $\Delta\varepsilon'$ values ~~have~~ exhibit a large-scale tendency to decrease with increasing depth and the data show more~~. The~~ scatter ~~of the raw data tends to be larger~~ at greater depths. Below 2900 m, the $\Delta\varepsilon'$ values largely fluctuated.

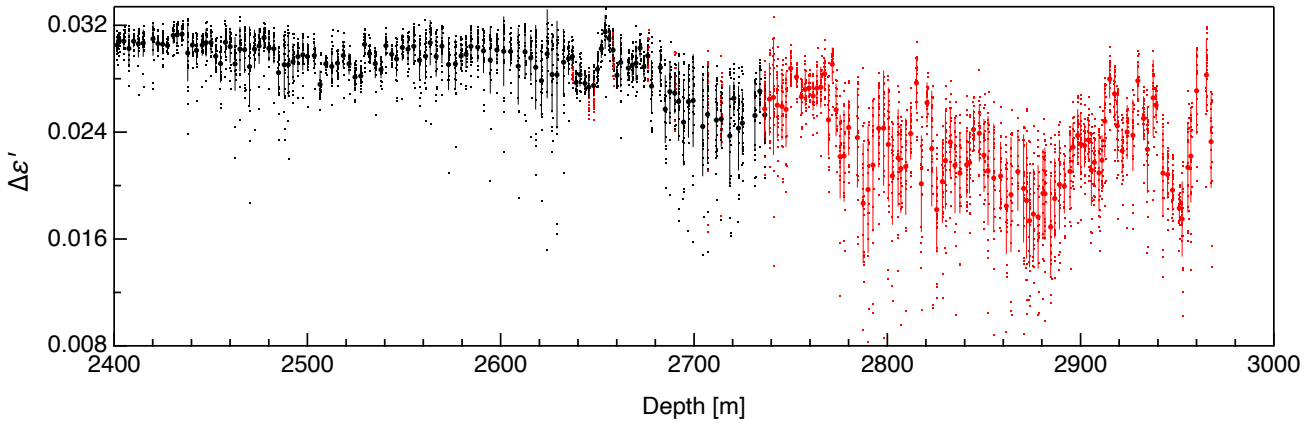

Figure 3. The $\Delta\varepsilon'$ data generated in this work. ~~in the LO20%~~. Dots represent raw data~~, recorded~~ acquired at every 0.02~~-m step~~ intervals. ~~Markers~~ Symbols and error bars indicate the ~~average~~ mean values and SDs for each 0.5~~-m step~~ intervals. Black and red markers/dots indicate data obtained without and with rotation of the samples in the open resonator, respectively (see Figure 2).

4.2 The *c*- and *a*-axis orientations measured by the Laue X-ray diffraction method

~~Figure 4 presents examples of the *c*- and *a*-axis orientations obtained through the Laue measurements. Examples from 17 of the 42 measured depths are shown. The three panels, from left to right (views from 1 to 3), represent *c*- and *a*-axis projected on the Schmidt equal net diagram as follows. View 1: Horizontal view from the axis of the microwave beam incidence (the center of the diagram), which is the same view as in Figure A2b in Supplementary Information A2, without information of the inclination angle or the horizontal orientation of the *c*-axes cluster. View 2: Horizontal view from the orthogonal direction (axis) of the inclination angle. This view is attained by horizontal rotation of the system using the vertical axis, by moving the center of the *c*-axes cluster to the periphery of the diagram. This operation relates to the horizontal orientation. The center of the diagram is parallel to the girdle of the *a*-axes. This view corresponds to that in Figure A2b'. View 3: View seen from the center axis of the *c*-axes cluster. In all diagrams, red dots and dark blue dots represent the orientations of *c*-axis and *a*-axis within the space, respectively. Additionally, green triangle markers indicate the orientation of the vertical in the ice sheet. The fourth column (View 4) indicates normalized density ρ of the *a*-axis along the girdle plane of the *a*-axis. θ (degrees) is angle from the figure top of the View 3.~~

The *c*- and *a*-axis distribution data obtained from the Laue X-ray diffraction are given in Figure 4. The *c*–axis fabric was found to generally exhibit a ~~strong~~ significant single-pole cluster~~. The~~ the strength of ~~this cluster fluctuates~~ which fluctuated with increasing depth. ~~Since~~ Because each crystal grain in the hexagonal crystal lattice had three equivalent *a*-axes orthogonal to the *c*-axis, the distribution of the *a*-axes formed a girdle plane orthogonal to the *c*-axes cluster at each depth. ~~As for the inclination angle,~~ The angle of inclination was found to increase monotonically larger at greater depths down to 2967 m. Figures 4(m–q) display data from the deepest five depths, ~~which lie~~ all of which were within the bottom 2% of the ice sheet. ~~At each depth,~~ In these figures, the red and blue numerical markers indicate the distributions of the *c*-axis and *a*-axis,

respectively, at each depth. As a consequence~~. Because of~~ grain growth near the bed of the ice sheet, the largest number of no more than six crystal grains were found in a thin section~~ was six. Therefore,~~ and the centre of the clusters could not be determined with this very limited number of grains. ~~Except~~ With the exception of these five depths, both the angle of inclination ~~angle~~ and the horizontal orientation of the *c*-axes cluster could be ascertained based on analysis of the *c*-axis ~~were extracted through the observation of *c*-axis~~ fabric, ~~considering~~ as shown by View 1 to 3. ~~views from 1 to 3.~~ Both these factors were subsequently used ~~for the corrections from~~ to correct $\Delta\varepsilon'$ values to $\Delta\varepsilon$ data and the procedure used for these corrections is detailed ~~We present correction procedures~~ in Supplementary Information Section 2. ~~In addition, the~~ The median inclination of the *c*-axes cluster values was also calculated using the thin-section-based *c*-axis fabric data acquired from thin sections. Both the angle of inclination ~~angle~~ from the vertical and median inclination values for the *c*-axes cluster are presented in Figure 5f. The angle of inclination of the *c*-axes cluster was found to increase monotonically at greater depths down to 2967 m.

The *a*-axis fabric generally exhibited pronounced ~~exhibits a strong~~ girdle-type clustering on each plane. ~~As with the fluctuations of~~ Similar to the *c*-axis cluster data, the strength of this girdle clustering fluctuations varied ~~fluctuates~~ with increasing depth as well. Because each grain had ~~of the~~ three equivalent *a*-axes orthogonal to the *c*-axis for each crystal grain, the distribution of the *a*-axes in a girdle plane ~~generally have periodicity of~~ typically displayed maxima at 60° intervals. ~~We find in depth dependent~~ The depth profiles in View 4 indicate that the normalized density, ρ, of the *a*-axis along the girdle plane of the *a*-axis exhibits a variable relationship with ~~strong inhomogeneity being dependent on~~ θ. In some cases, there are significant variations at ~~it indicates strong~~ 60°~~periodicity~~, intervals, as can be seen in Figure 4b, 4e and 4g. ~~and several more examples in the Supplementary Information A Section 4. In other cases, there are super positions of it indicates superposition of variations with such 60° variations periodicity such as in Figure 4a, 4c, 4h and 4k. examples are (a), (c), (h), and (k) in Figure 4. We discuss these clusters of the *a*-axes in this paper.~~

~~Distribution of~~ The *c*-axes distribution of each thin section and the *a*-axes ~~anisotropy~~ inhomogeneity are ~~further shown~~ also presented in Figures 5c and 5d. ~~In terms of the distribution of *c*-axes, we can find crystal grains with *c*-axis oriented around~~ Crystal grains having a *c*-axis orientation I the range of 30°–60° were found at depths below 2600 m, ~~in particular, except for~~ with exception of the impurity-rich layer indicated by brown shading. Here the term impurity-rich means that the ice contains either insoluble particles (like dust) and/or soluble impurities such as dissolved ionic species. The *a*-axes ~~anisotropy~~ inhomogeneity was defined as the SD of the *a*-axes density, ρ, (hereinafter, SD_ρ) as shown in panels View 4 in Figure 4. Here, larger values correspond to more anisotropic ~~distribution of~~ *a*-axes distributions. ~~We find that there are~~ The data demonstrate relatively small and large extent of ~~anisotropy~~ inhomogeneity in the impurity-rich layers and impurity-poor layers, respectively, and show that the SD_ρ of the *a*-axis ~~anisotropy~~ inhomogeneity ~~exhibit~~ undergoes large scale fluctuations associated with ~~changes~~ transitions between glacial and interglacial periods. It is also very important to note that the SD_ρ ~~is well synchronized~~ data appear corrected with the grain size (Figure 5e).~~, which implies underlining Physics~~.

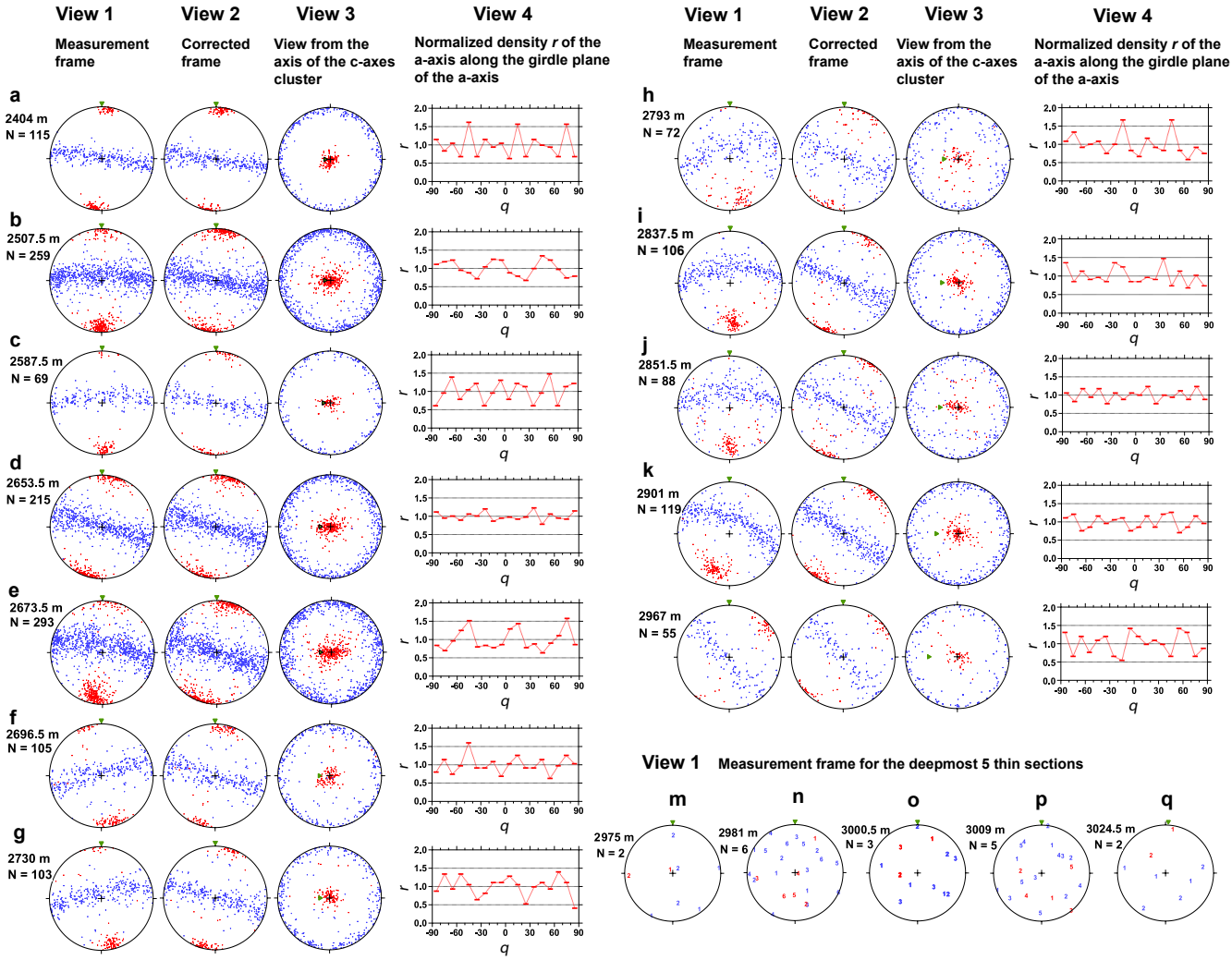

Figure 4. The *c*-axis distribution data and *a*-axis distribution data obtained from the Laue X-ray diffraction ~~measurements.~~ analyses using 17 depths ~~were selected from~~ out of a total of 42.4a to 4I present data for the 12 shallower depths over the ~~At each depth of the shallower 12 depths from (a) to (l) in depth~~ range of 2400 and 2967 m in the form of ~~, we show three Schmidt equal area~~ three equal area Schmidt net diagrams (e.g., Langway, 1958). These diagram s summarize the projected ~~to express the distributions of~~ *c*-axis and *a*-axis distributions as indicated by ~~projected on it with~~ red and blue ~~colors for~~ symbols/markers, respectively. For these 12 depths, the ~~left diagram (view 1) is the projection~~ leftmost diagram (View 1) show projections from the measurement frame (refer to Figure S2b while the ~~). The~~ second series of diagram (View 2)~~left diagram (view 2) is the~~ is a projection from the corrected frame (see Figure S2b'). The third ~~left~~ series of diagram (View 3) is a projection from the centre of the *c*-axes cluster. The green triangle in each diagram indicates the vertical orientation in the ice sheet, which~~. The vertical orientation~~ approximately aligns with the core axis (though the borehole inclined 3–6° from the vertical). The fourth column contains plots of the ~~indicates~~ normalized density, ρ, of the *a*-axis along the girdle plane of the *a*-axis against θ (in degrees) which is the angle from the figure top of the figure in View 3. ~~Diagrams from (m) to (q)~~ The figures in 4m to 4q show projections ~~represent the projection~~ from the measurement frame for the deepest five depths, ranging from 2975 to 3024.5 m. Because of grain growth near the bed of the ice sheet, each thin section contained less than six grains Rather than dots, numerical markers are used to indicate the orientation of each grain. ~~number of crystal grains in each thin section was less than 6. Instead of dots, number markers were used to indicate the orientation of each grain.~~

4.3 Depth-dependent variations of corrected Δε and SD values, and eigenvalues

~~We corrected from~~ In this work, Δε′ values were corrected to Δε data using both the angle of inclination ~~angle~~ and the horizontal orientation of the *c*-axes cluster as estimated from the Laue X-ray diffraction method. The correction procedure ~~are presented~~ is described in Supplementary Information Section 2. Figure 5a ~~indicates~~ plots the corrected Δε values and eigenvalues obtained ~~from~~ using the Laue X-ray diffraction process ~~method~~. As was also the case in ~~with the~~ Figure 3, ~~markers~~

the symbols and bars here indicate the ~~average~~ mean values and the SDs determined at 0.5-m intervals along the core sample. Assuming a single-pole fabric without horizontal anisotropy, the ~~The~~ relationship between the $\Delta\varepsilon$ and eigenvalue data can be ~~is~~ expressed as $a_3^{(2)} = (2\Delta\varepsilon / \Delta\varepsilon_s + 1) / 3$, ~~assuming a single-pole fabric without horizontal anisotropy. Here,~~ where $\Delta\varepsilon_s$ is ~~represents~~ the dielectric anisotropy of a single crystal. The $\Delta\varepsilon$ values (Figures 5a) reached a maximum of ~~reaches~~ approximately 0.031 at depths of 2430 and 2654 m and then proceeded to exhibit significant fluctuation. The evident~~. After reaching this maximum level, the $\Delta\varepsilon$ values fluctuate largely. The~~ decrease in $\Delta\varepsilon$ values and increase in the SDs are a direct consequence of ~~larger SD are directly linked to~~ the scatter in the individual $\Delta\varepsilon$ measurements (represented by the dots in Figure 5a). In the case that this ~~When scatter~~ is pronounced, the mean $\Delta\varepsilon$ value ~~averaged over each~~ for a 0.5 m segment becomes smaller and the SD larger. At depths greater than ~~about~~ approximately 2900 m, the $\Delta\varepsilon$ values exhibit greater fluctuations over distances on the order of 10 m. It should also be is noted that when the SD values are large, $\boldsymbol{\Delta\varepsilon}$ for each ice core specimen show large ~~displays numerous sharp~~ negative spikes in conjunction with large SDs, ~~$\Delta\varepsilon$, as shown~~ as demonstrated by the dots in the panel and ~~an example~~ the typical profile presented in Figure S9.

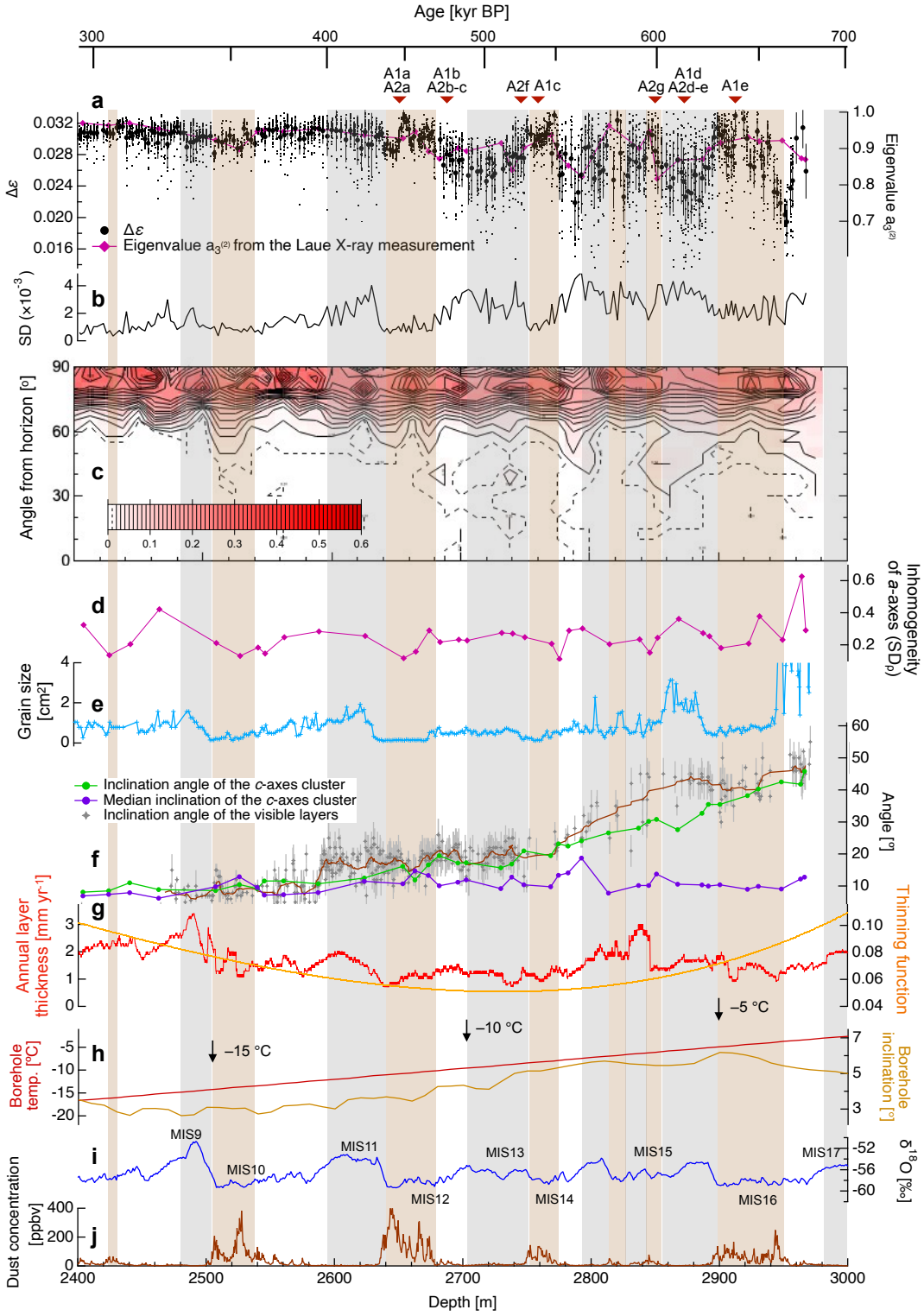

Figure 5. A detailed comparison of Δε values with various ice core data ~~in the LO20%~~. (a) Δε (mean and raw data generated using the ~~from~~ DTM) and eigenvalues (from the Laue X-ray diffraction method). The potential uncertainty in the eigenvalues based on the total number of ~~sampled~~ grains sampled is discussed ~~are given~~ in Supplementary Information Section 1.4. (b) SD values. (c) The distribution of *c*-axes as angles ~~from~~ relative to a plane orthogonal to the *c*-axes cluster at generated ~~. This was analysed~~ using the data obtained from the Laue X-ray diffraction method. The probability of the presence of *c*-axes in a given region is shown by the ~~is expressed with~~ contour lines. (d) The inhomogeneity of the *a*-axes as demonstrated by the SD of the ~~shown as standard deviation of~~ *a*-axes density, ρ ($SD_ρ$). (e) Grain size data. (f)The angles of inclination of the *c*-axes cluster and the layered determined by visual observations ~~visual layers (smoothing)~~ together with median inclinations. The orange line was generated by smoothing of the angle of layers at ten measuring points. (g) Data showing annual variations in the ~~Annual~~ layer thickness and thinning function (DFICPM, 2017). (h) Borehole temperature and inclination data (Motoyama et al., 2020). (i) $δ^{18}O$ data (DFICPM, 2017). (j) Concentrations of dust particles (DFICPM, 2017). Gray and brown shading indicate

interglacial periods and depths ~~with a~~ having higher concentrations of impurities (~~representing~~ that is, impurity-rich layers), respectively. The depths at which ~~we observed the~~ microstructure were observed are indicated in the upper part of the figure.

4.4 Grain sizes, ~~and~~ layer inclinations, and microstructures

~~The results for the grain sizes~~ The grain size and inclination data for angle of the visible layers are presented in Figures 5e and 5f, respectively. The grain sizes associated with interglacial and glacial periods were found to be significantly larger and smaller, respectively. ~~tends to be larger during interglacial periods and significantly smaller during glacial periods~~, with this difference becoming more pronounced at greater depths. It is also apparent that the ~~We observed that~~ $\Delta\varepsilon$, the SD values for $\Delta\varepsilon$ data and the grain sizes were approximately synchronous implying the presence of a common underlying factor. The grain sizes exhibited no overall increase trend with increasing depth. ~~we could observe only weak increasing trend versus depth.~~ The grain sizes at depths between 2900 and 2950 m remained small despite temperatures higher than –5 °C in this region. ~~At~~ However, at depths greater than ~~2950~~ 2960 m (equivalent to ~~in~~ the deepest approximately 2% of the core), the grain sizes were extremely large, often reaching sizes in excess of 300 cm^2. The grain size data acquired below 2950 m are shown in Figure 6. ~~Grain size profile within the entire thickness is displayed in Figure 10e along with the grain size reported from the UP80% of the DF1 ice core (Azuma et al.1999, 2000). We observe that in the UP80%, the grain size increased steadily, while in the LO20%, the grain size tends to fluctuate, showing~~ The sizes can be seen to have fluctuated and there is a clear distinction between the very small grains in the impurity-rich layers and the larger grains in the impurity-poor layers. ~~There is a transition of the data aspect at depth of about 2500 m.~~

~~The inclination angle of the visual layers will not be exactly consistent with the inclination angle of the *c*-axes cluster if simple shear strain occurs in the ice sheet. The simple shear in principle contains components of compression, extension, and rigid-body rotation of the system. In this case, an axis orthogonal to the shear plane and the inclination angle of the *c*-axes cluster will deviate. Indeed, We Furthermore, we observed that the inclination angles of the *c*-axes cluster and visual layers deviate over a wide range of depths, deeper than about 2580 m (Figure. 5f). The deviation is pronounced at depths between 2800 and 2900 m.~~ The inclination angle of the visual layers (see orange line in Figure 5f) shows stepwise changes at 2580 and 2770 m, being 10° at depths less than 2580 m, 20° at 2770 m, and reaching 45° at 3000 m. The present data demonstrated that the angles of inclination of the *c*-axes cluster and of the visual layers deviated over a wide range of depths below approximately 2580 m (Figure. 5f). This deviation was most pronounced at depths between 2800 and 2900 m.

Microstructural observations demonstrated the difference of manner concerning dynamic recrystallization and the crystal morphology between the impurity-rich and impurity-poor layers. Evidence of migration recrystallization, such as bulged grain boundaries and interlocking grains, as well as potentially nucleated grains, were found in impurity-poor layers. Detail of the microstructures is given in Appendix A.

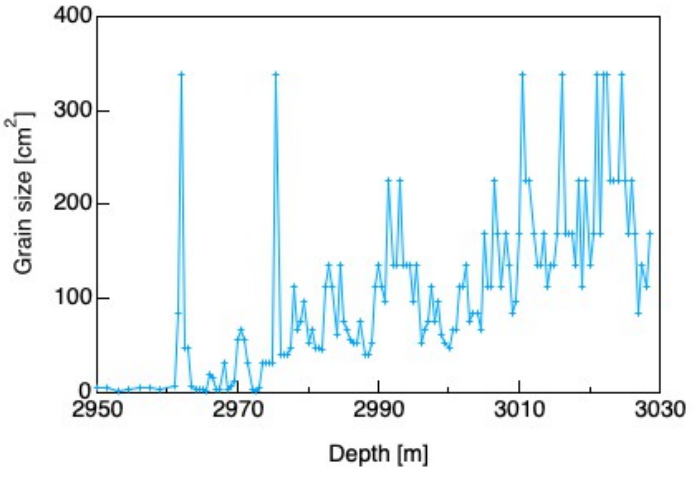

Figure 6. Grain size data acquired below 2950 m. Note that the scale of the vertical axis is significantly different from that in Figure 5e.

5. Discussion

~~**5.1 Variations in the layer structures in the deeper sections**~~

5.1 Development of crystal orientation fabric and layered structures in the deep sections: common and unique features of the site

~~Due to the prevailing temperature and stress conditions, the ice within the Antarctic ice sheet(s) is located in a boundary zone between dislocation and diffusional creep on the deformation mechanism map The conditions of ice sheets in Antarctica, in terms of temperature and stress, are located on a boundary zone between dislocation and diffusional creep on the deformation mechanism map (e.g., Shoji and Higashi, 1978; Goodman et al., 1981, Duval et al., 1983). When ice is at under At temperatures close to its melting point in the LO20%, the viscosity of ice is lower, reduced and diffusion coefficients are higher compared with those of to the colder ice. The rate at which recrystallization occurs also increases with temperature (e.g., Petrenko and Whitworth, 1999). Regarding the stress field, the~~

~~We compared the~~ The relationship between $\Delta\varepsilon$ values and normalized eigenvalues, $a_3^{(2)}$, and grain sizes in the DF and EDC ice cores were examined (Figure 7). These two sites are similar in terms of glaciological conditions, including surface temperature, annual mean surface mass balance and ice thickness (EPICA Community Members, 2004; DFICM, 2017). In addition, the dust flux profiles of the DF and EDC ice cores are very similar (DFICPM, 2017). The general trends exhibited by ~~in~~ cluster strength and grain size were found to be close to equivalent ~~are very similar~~ in both ice cores. Surprisingly, the *c*-axes cluster strength in the DF ice core was almost the same as that in the EDC ice core, even though the layer structures in the DF were largely inclined. Hence, layer inclination via rigid body rotation appears not to affect the cluster strength. ~~Furthermore,~~ Durand et al. (2009) pointed out similar depth-dependent developments in *c*-axis clustering in deep sections ~~are similar in~~ of the GRIP ice core (Thorsteinsson et al., 1997) and the EDC core in Antarctica. The ~~similarity~~ equivalency among these three sites across both hemispheres implies that certain physical mechanisms are driving this similar development of *c*-axis clustering. ~~We~~ The authors propose ~~hypothesize~~ that the ambient temperature environment within these ice sheets could have produced this effect through mechanisms such as dislocation creep and recrystallization. At depth of approximately 2400 m, the thickness of the ice was close to ~~might have resulted in the commonality of *c* axis fabric. At around 2400 m, the thickness of ice is approximately~~ 10% of the original ice equivalent thickness at the time of deposition (see Figure 5g)~~. At this depth~~, ~~where the eigenvalue~~ with an eigenvalue, $a_3^{(2)}$ ~~reaches about~~ of approximately 0.93. A highly clustered texture is unlikely to form in the case of zero or minimal shear stress as a means of compression or shear, such that dynamic recrystallization occurs as an accommodation process. ~~In the absence (or faint presence) of shear stress, a strongly clustered texture will be difficult, either to compress or shear, thereby necessitating dynamic recrystallization as an accommodation process.~~ This state of saturation of the *c*-axis cluster, along with the common temperature range may be more effective triggers for ~~as a condition to trigger~~ nucleation and recrystallization. The deepest 10–20% of the polar ice sheets is typically characterized ready deformation in response to horizontal shear because of the presence of ~~by their ability to easily deform under horizontal shear, due to~~ high temperatures and ~~well-clustered~~ a highly clustered *c*-axis fabric. At these depths, dynamic recrystallization plays a critical role, particularly in impurity-poor layers, ~~to recover the potential~~ in the recovery of various *c*-axis orientations ~~available~~ capable of promoting deformation based on dislocation creep. ~~for the continuation of dislocation creep based deformation.~~

A unique feature of the DF ice core is the inclined layered structures. The coring site is situated on a bank very close to a subglacial trench (Figure 1c) with both difference and distance between the two being~~. Between the subglacial trench and the coring site, the depth difference and distance are each~~ approximately 100 m. This geometry corresponds to the maximum

~~inclination~~ angle of inclination of the *c*-axes cluster of approximately 45° and the angle of inclination ~~angle~~ of the ~~visual layers~~ visually-identifiable layers of approximately 45° near the base of the ice sheet (Figure 5f). ~~In addition, the~~ This deeper trench may act as a pathway for the flow of subglacial water ~~and~~ while the deeper bed can accumulate meltwater ~~is a location for more melt~~ (e.g., Pattyn, 2010, Fujita et al., 2012). Thus, ~~we~~ the authors suggest ~~hypothesize~~ that ~~there is~~ a simple shear strain component is directed towards the subglacial trench. The rheology of polycrystalline ice with a single-pole fabric is ~~like~~ similar to that of the single crystal ice, in that both will readily deform in response to simple shear stress. ~~It easily deforms under simple shear stress. The authors suggest that the simple shear stress dominates the deformation of ice at the bottom part of DF.~~ In the case of DF, because of the friction force between ice and inclined bedrock, simple shear system would rotate the entire system including the internal layers and the *c*-axes cluster together. In principle, simple shear is a superposition of pure shear and the rigid-body rotation of the system~~. The~~ and layer inclination ~~is~~ can be simply caused by the system's rigid-body rotation. ~~Figures 8d and 8e illustrate 2D schematic explanation for configuration of strains and rotations in the ice body above the steep bedrock slope and near the bedrock.~~ The *c*-axes also are included within the system's rigid-body rotation. ~~However, the cluster of the *c*-axes alone will rotate backward due to the compression components within the pure shear by dislocation creep.~~ However, normal components of the strain (both compression in the near-vertical and extension near the horizontal plane) causes the rotation of *c*-axes cluster alone toward the vertical by intracrystalline slip at the same time. In this way, total amount of inclination becomes larger for the layers than the *c*-axes cluster. Thus, the ~~inconsistency of~~ mismatch between the angles ~~is the evidence~~ implies that ~~for dominance of the~~ simple shear was the primary mechanism within this depth range. ~~Such features were not reported in the EDC ice core. This implies that these features are due to an environment specific to DF.~~ Considering the consistency of the eigenvalues between the DF and the EDC ice cores (Figure 7), the rigid-body rotation appears not to affect cluster strength. The nature of deep sections in the DF ice core is similar to that of EDML ice core (Weikusat et al., 2017), which is located in a divide region, where horizontal flow occurs. In the deepest sections, strong shear stress parallel to the bedrock predominant is predominant. In contrast, the DF ice is located within a dome region. Even in the case that vertical compression is predominant in shallow sections, shear stress may be the primary mechanism in deeper sections due to the bedrock inclination at the deep sections.

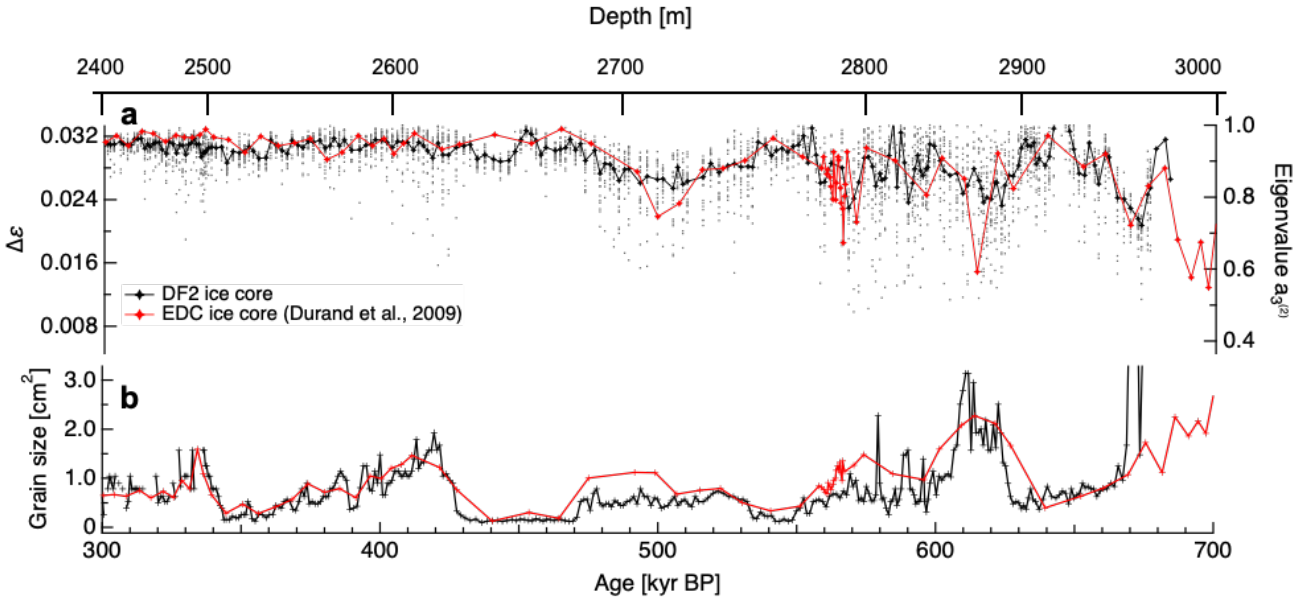

Figure 7. A comparison of the *c*-axis fabric and grain size data obtained from the DF2 core and the EDC core, applying the AICC2012 age scale (Bazin et al., 2013). (a) Δε presented as raw data (dots) and as mean values for each 0.5 m segments (black symbols for DF data) or for each thin section (red symbols for EDC data). The right-hand axis provides a scale for normalized eigenvalues. (b) Grain sizes in the DF and EDC cores. The EDC data are obtained from Durand et al., 2009.

5.2 Relationships between the *c*-axis fabric and layer structure parameters

Figure 5 illustrates the relationships between *c*-axis fabric, layered structures, and physicochemical properties. The figure plots (a) Δc (mean and raw data from DTM) and eigenvalues (from the Laue X-ray diffraction method), (b) SD values, (c) the distribution of *c*-axes relative to a plane orthogonal to the *c*-axes cluster, (d) *a*-axes anisotropy within the girdle, (e) grain sizes, (f) inclination angle of the *c*-axes cluster and the visual layers, and median inclination, (g) the annual layer thickness and thinning function, (h) borehole temperature and inclination, (i) $\delta^{18}O$, and (j) concentration of dust particles. The relationship between *c*-axis fabric and layered structures evolves with increasing depth (Figures 5a–5f). Schematic diagrams of the relationships between layered structures and orientation of *c*-axes cluster are shown in Figures 8(a–c). The angle of inclination angles of the visually identifiable layers and the of *c*-axes cluster were approximately consistent at depths shallower than about above approximately 2600 m (Figure 5f). This finding indicates that the overall system, composed of the visible layers and the *c*-axes cluster, rotated together as a rigid body. At depths below this point deeper than about 2600 m, the agreement between the angles of inclination of the visual layers and the *c*-axis cluster was affected by the varying conditions experienced by ice deposited during the glacial and interglacial periods. the consistency of the inclination angles in the visual layers and the *c*-axes cluster depends on glacial/interglacial periods. In the case of samples associated with In glacial periods (MIS12, 14, and 16), both angles are approximately consistent, whereas in the interglacial periods (MIS11, 13 and 15) they are not. Specifically, the angle of inclination angle of the *c*-axes cluster is smaller than those of the visual layers. This implies that the crystal grains undergo underwent a simple shear mechanism, with less rotation rotating less than layer structure rotation in these depth ranges, particularly during interglacial periods.

Next, we discuss Here, it is also helpful to assess layer thinning. DFICPM (2017) analyzed the thinning function (the ratio of the ice layer thickness to its initial thickness at the surface) of the DF2 core from the depth sequence of the climate signals and annual layer thickness (see Figure 5g). The thinning function was found to decrease decreased to a local minimum at about approximately 2750 m and then increase again at greater depths. The authors hypothesized that spatially inhomogeneous basal melting might have been associated with be linked to this anomalous thinning. In Figure 5g, a broad local minimum of the thinning function is located at 2700–2800 m. This depth is in good agreement with the depth at which the large disagreement between the angle of range agrees well with starting depths for large inconsistency between the inclination angles of the *c*-axes cluster and the inclination angles of the layers began. Importantly, this depth is also the approximate starting point for the increased fluctuations boundary where larger fluctuation of the Δc values started. It may be We speculate that the observed phenomena are linked to higher temperatures, and thus to the activated occurrence of recrystallization, as well as to and increased strain resulting from of simple shear from generated by the bed. Then, we propose a scenario for development of the layer structure at the deeper part in DF based on the observed data using Figure 8f. An important point is that It is important that the DF drilling site is located just above a subglacial slope at the bank of a meltwater drainage pathway (Tsutaki et al., 2022). Under the dominance of the vertical normal stress With vertical normal stress being dominant near the dome, horizontal shear appears primarily on the subglacial slopes rather than ridges or troughs (Tsutaki et al., 2022). Basal troughs are also often influenced affected by basal melt or are connected to deeper troughs containing of more basal melt. Consequently, such troughs tend to serve as rapid pathways for ice flow. Thus, we the authors suggest that the subglacial slope near the trough causes ice to flow towards the centre of the trough, thus applying shear force to the layers. shearing the layered conditions. Furthermore, spatially Spatially inhomogeneous basal mass loss resulting from due to melting could also lead to an imbalance in force equilibrium in the vertical direction. Below the hardest ice, ice mass is lost locally at the base and . As a result, layers can consequently be stretched downwards, creating a convex shape centered around the location of the trough.

5.2 Large-scale development in the crystal orientation fabric and grain sizes: variations during the glacial/interglacial periods

~~Within the UP80%,~~ A clear advantage of DTM is that data with high sampling, spatial resolution and continuity allowed for the evaluation of *c*-axes cluster fluctuations in comparison with various ice core data. Saruya et al. (2022b) investigated the ~~controlling~~ factors affecting the ~~of~~ *c*-axis fabric at depths above 2400 m by assessing correlations between ~~by comparing~~ $\Delta\varepsilon$ and ~~with~~ various ionic impurities and dust concentrations. They found that $\Delta\varepsilon$ exhibited a positive correlation ~~is correlated positively~~ with the concentration of Cl^- ions but an inverse correlation ~~and inversely~~ with the amount of dust particles. In contrast to depths above 2400 m, ~~UP80%,~~ the relationship between $\Delta\varepsilon$ and Cl^- ions ~~within the LO20%~~ was unclear below 2400 m. ~~For the depths of the LO20%, we~~ This work compared $\Delta\varepsilon$ with $\delta^{18}O$, grain size, and dust particle concentration (Figure 5). ~~Profiles of concentration of ionic impurities (Cl^-, SO_4^{2-} and Ca^{2+}) are plotted in entire depths figure (Figure 10).~~ Referring to the $\delta^{18}O$ profile, ~~we observe~~ it is apparent that ~~depressions in~~ the mean $\Delta\varepsilon$ values decreased (caused by the large scatter of data points) occur during interglacial periods at depths below ~~2650~~ 2640 m. These decreases became more pronounced as the ~~the depressions deepen with larger~~ scatter of the raw data became more significant at greater depths. The ~~relative sizes of~~ SDs were smaller samples associated with glacial periods and larger during interglacial periods~~, respectively~~ (Figures 5b). High concentrations of ~~The highly concentrated~~ impurities had an apparent ~~influence~~ effect on the $\Delta\varepsilon$ values, maintaining ~~a persistently~~ consistently high level of $\Delta\varepsilon$ below 2600 m (Figure 5a). ~~Additionally, grain sizes tend to be small~~ Small grain sizes were also present (Figure 5e).~~, and the aspect ratio of the crystal grains remains consistently high in these layers, with values reaching up to 2 (Figure 9).~~ Overall, ~~these textural features —~~ the grain sizes ~~and morphologies~~ together with the~~, shapes, and~~ *c*-axis fabric~~— are~~ were found to be interdependent and strongly correlated with the presence of impurities.

Above 2400 m, the grain size grew steadily (but with a partial decrease during the two glacial periods) (Azuma et al., 1999, 2000). However, below 2400 m, there was no overall increase in grain size. During interglacial periods, the grain size gradually increased with depth but decreased sharply during glacial periods that were associated with higher impurity concentrations. At the lower glacial ice boundary, the grain size again became smaller, indicating that grain size growth was interrupted during glacial periods. This pattern has also been reported to occur in the EDC core (Durand et al., 2009). The reason why grain growth in deeper ice is interrupted during glacial periods remains unclear, although this effect may be due to nucleation or migration recrystallization. Figures 5c and A2 show signs of nucleation and migration recrystallization, both of which can reduce the mean grain size, in interglacial ice specimens. These phenomena may suppress normal grain growth and lead to smaller grain sizes. Furthermore, extremely large grains exceeding 10 cm in radius (~300 cm^2) were observed below 2960 m. Grains of this size have not been found in the EDC core to date (see Figure 7). Interestingly, small grains (less than 1 cm^2) were maintained at a depth of approximately 2900 m (MIS16), despite the high temperatures at that depth that were close to the melting point of ice (-5 °C). Although the concentration of dust particles was not so high in this region (less than 100 ppbv), the grain boundary pinning effect caused by dust particles remained still effective even at high temperatures.

Significant changes in the cluster strength and the distributions of *c*-axes angles were found below the impurity-rich layer at depths between 2640 and 2680 m. The fluctuations in $\Delta\varepsilon$ values increased significantly and the crystal grains having a *c*-axis orientation in the range of 30°–60° appeared. The reason for these changes remains uncertain, but one possible explanation is the activation of migration recrystallization. Migration recrystallization is thought to occur at temperatures higher than –10 °C. (e.g., Duval and Castelnau, 1995; Montagnat et al., 2009). The ambient temperature at this layer is approximately –10 °C. The authors propose that the activation of migration recrystallization caused these changes, and the dusty impurities that influences the grain boundary mobility are responsible for the degree of this process.

5.3 Impacts of dust particles and dynamic recrystallization on the crystal orientation fabric and grain sizes

The behaviour of dynamic recrystallization highly depends on the temperature and impurities (e.g., Humphreys and Haterly 2004; Cuffey and Paterson, 2010). It should be also noted that the relationship between cluster strength and the concentration of dusty impurities changes at approximately 2640 m. According to a case study ~~for~~ concerning the NEEM ice core by Eichler et al. (2017) and a review by Stoll et al. (2021b), dust particles are located not only at grain boundaries but also in grain

interiors and at triple junctions. ~~To the best of our knowledge,~~ It is well known that dust particles restrict grain growth and result in smaller grain sizes (e.g., Alley and Woods, 1996); however, the role of dust particles in ice deformation via dislocation creep)is not well understood. Dust particles can product dislocation; ~~Production of dislocation is one of the possibilities. in contrast,~~ or ~~microparticles~~ may act as sink of dislocation like grain boundaries. Saruya et al. (2022b) suggested two ~~possibilities:~~ possible actions of particles: (i) restricted deformation due to the inhibition of dislocation by dust particles and/or (ii) the ~~contribution~~ promotion of diffusion creep that does not cause *c*-axis rotation. Diffusion creep is known to be promoted by smaller grain sizes.~~because, with this mechanism, only molecules diffuse due to the condition of smaller grains.~~ Which of these effects ((i) or (ii)) is more dominant is not currently known although ~~remains unresolved. However, in either case,~~ either one could ~~they can~~ restrict ~~changes in~~ the *c*-axis clustering. ~~What we observed in ice below about 2600 m is~~ The present work found that the degree of *c*-axis clustering in the dusty (i.e., impurity-rich) layers containing dust below 2600 m was stronger than that in the surrounding layers. This trend cannot be explained by the above two possibilities. Additionally, the consistently smaller grain sizes ~~and higher aspect ratios of the crystal grains~~ in the impurity-rich layers indicate that grain boundary migration was also restricted in such ice. This confirms that the movement of dislocations (as line defects) and of grain boundaries (as planar defects) within the crystal lattice ~~is significantly influenced~~ was greatly affected by the presence of ~~insoluble impurities~~ dust particles that act as obstacles.

~~Comparing the relationship of *c* axis fabric with impurities in the UP80% with the LO20%, in the UP80%, impurity-rich/poor layers have smaller/larger Δc values. In the LO20%, some thickness between 2400 m and 2650 m is a kind of transition zone; in it we find no clear correlation between Δc values and impurity. Below depths of about 2650 m, the trend is seemingly reversed. The *c*-axis fabric clustering strength exhibited substantial fluctuations. There, more impurity-rich layers maintain clustering persistently. In impurity-poor layers, relaxation of the *c*-axis fabric clustering occurred, as represented by numerous negative spikes of Δc. A similar relationship exists between the aspect ratio and impurities in the UP80% and LO20% sections. In Figure 9, we observe an increasing trend in aspect ratio with depth in the UP80%. In contrast, the LO20% shows a distinct split in the data: an aspect ratio close to 2 in impurity-rich layers and much smaller values in impurity-poor layers.~~

~~In summary, the presence of insoluble impurities in the ice sheet had a significant impact on the *c*-axis fabric, grain size, and grain aspect ratio of crystal grains. Grain boundary migration was evidently restricted in In impurity-rich layers, particularly below 2600 m, grain boundary migration is restricted, leading to producing consistently smaller grain sizes and higher aspect ratios. The relationship between these textural features and impurities varies between the UP80% and LO20% sections, with a stronger correlation observed in the latter. These findings highlight the complex interplay between impurities and the deformation mechanisms within the ice, suggesting that the presence of insoluble particles plays a crucial role in controlling the microstructural evolution of deep ice.~~

~~5.4 Cause of *c*-axis fabric fluctuations inferred from microstructures~~

The *c*-axis fabric contains information ~~on several factors: (i)~~ concerning the deformational history~~, (ii)~~ of the ice as well as grain growth and ~~(iii)~~ recrystallization (e.g., Cuffey and Paterson, 2010; Faria et al., 2014a, b). Ultimately, all these factors are sensitive to the deposition of insoluble impurities~~. Insoluble impurities restrict~~ that limit grain boundary migration through Zener pinning mechanisms and also impede dislocation movement (Alley and Woods, 1996; Durand et al., 2006). ~~These characteristics result in slow growth of *c* axis clustering in impurity rich layers within the UP80% and slow relaxation of *c*-axis clustering in the LO20%. This leads to an apparent reversed correlation between Δc values and impurity levels in both the UP80% and the LO20%. In terms of the distribution of *c*-axes (Figure 5c), we can find crystal grains with *c*-axis oriented around 30–60 degrees at depths below 2600 m. It is believed that new grains tend to form with an orientation favorable for basal glide~~ The distribution of *c*-axes shown in Figure 5c indicates that crystal grains having a *c*-axis orientation in the range of 30°–60° appeared at depths below 2600 m. New grains are thought to have been formed with an orientation that promoted basal glide (e.g., Alley, 1992; Humphreys and Hatherly, 2004, Cuffey and Paterson, 2010), ~~that is,~~ meaning approximately

45° from the compressional axis. ~~However, it is also noteworthy that, in Figure 5c, distribution of *c*-axis density approximately from 30 degrees from compressional axis (60 degrees from horizon) is always denser than 45 degrees or 60 degrees. It is possible that it has some underlying mechanisms in terms of nucleation recrystallization relative to the existing *c*-axis cluster. Additionally, crystal grains with *c*-axis oriented around 30–60 degrees tend to appear more in the impurity-poor zones where grain size is larger with low level of Δε. We suggest that these grains with a *c*-axis orientation of around 30–60 degrees represent nucleated grains in the deeper part, and that these grains might grow and eliminate old grains by migration recrystallization. At the same time, ice crystals will develop c-axis orientations favorable for ice crystals will recover the *c*-axis orientations available for the continuation of dislocation creep based deformation. The hypothesis that these grains are the result of nucleation is consistent with the observation of the corresponding grains, as described in Section 4.5.~~ Additionally, crystal grains having *c*-axis orientations in the range of 30°–60° were more frequent in the impurity-poor zones, in which the grain size was larger and the Δε values lower. The authors propose that these grains with a *c*-axis orientation of 30°–60° correspond to nucleated grains in the deeper part of the ice and could have grown while eliminating older grains by migration recrystallization. These ice crystals would be expected to develop *c*-axis orientations that favoured dislocation-creep-based deformation. The formation of such grains as a result of nucleation is consistent with the observations of the corresponding grains.

Concerning the *a*-axes organization, in the case that the degree of inhomogeneity of the *a*-axis within the girdle was expressed as SD_p, these values were generally larger in impurity-poor layers and smaller in impurity-rich layers (Figure 5). Thirdly, the SD_p values and grain size were approximately synchronous (Figures 5). During dislocation creep, if the basal plane is the primary slip plane (that is, the easy-glide plane of hexagonal ice), it is unlikely that *a*-axis organization will occur geometrically on this basis. Since dislocation creep and a-axis organization do not seem interdependent, we can exclude this possibility. The organization of the *a*-axis structure among the crystal grains can occur as a result of interactions at the boundaries between adjacent grains. Therefore, the authors speculate that dynamic recrystallization processes, particularly migration recrystallization associated with nucleation, play a critical role.

~~We~~ The authors propose that grain nucleation and migration recrystallization lead to significant changes in the crystal orientation fabric.~~; a~~The decrease ~~decreasing~~ in Δε values and less clustered *c*-axis fabric in impurity-poor layers can be explained by growth of the grains ~~with~~ having different *c*-axis orientations. Conversely, such grains were much smaller and limited in volume in the impurity-rich layers. Grain coarsening by migration recrystallization does not appear to occur because insoluble impurities restrict the grain boundary migration (e.g., Durand et al., 2006; Stoll et al., 2021b) ~~thus~~ and so limit the growth of the nucleated grains as well. Therefore, the changes in *c*-axis fabric ~~change~~ (meaning a decrease in ~~decreasing of~~ Δε values) caused by nucleation and migration recrystallization ~~would appear strongly~~ should be significant only in the impurity-poor layers. ~~Thus,~~ On this basis, the dynamic recrystallization process would be expected to greatly affect the ~~have greatly contributed to the characteristic behavior of~~ *c*-axis fabric development. Even in the case that ~~when~~ grain nucleation occurs in ice both in impurity-rich ice and in impurity-poor ice, the contribution of this process to changes in the *c*-axis fabric ~~changes~~ would depend on the surrounding conditions~~: it~~ Hence, this effect may not be immediately apparent in terms of the volume-weighted ~~average~~ mean Δε values obtained using ~~in~~ the DTM. However, ~~when such~~ the growth of these nucleated grains ~~grow~~, which occurs primarily ~~is the case mostly~~ in impurity-poor ice, and the subsequent strain-induced migration recrystallization could significantly affect the Δε values because of the growth of grains having different *c*-axis orientations. The influence of the migration recrystallization on the crystal orientation fabric at the deep sections in ice sheets has been also mentioned in the GRIP and EDC ice cores (Thorsteinsson et al., 1997; De La Chapelle et al. 1998; Durand et al., 2009),but the specific processes and contributions (such as differences in recrystallization activity between impurity-rich and impurity-poor layers, appearance of crystal grains having a *c*-axis orientation that was significantly offset from the surrounding grains, the mechanisms behind the relaxation and large fluctuations of *c*-axis clustering observed in the interglacial periods) were clarified in this work.

5.4 Small-scale development of crystal orientation fabric and grain sizes: fluctuations within impurity-rich and impurity-poor layers

Closeup profiles and scatter plot for $\Delta\varepsilon$ values, grain sizes and concentration of dust particles at depths between 2600 and 2820 m are given in Figure 9. The $\Delta\varepsilon$ values exhibit a negative correlation with dust particle concentration in impurity-rich layers but a positive correlation in impurity-poor layers (Figure 9d). A similar negative correlation has been also observed at depths above 2400 m (Saruya et al., 2022b), suggesting that the variation in $\Delta\varepsilon$ values within impurity-rich layers originated at shallow depths and was preserved until deep sections. In contrast, the variation of $\Delta\varepsilon$ values within impurity-poor layers appear to develop at greater depths due to the migration recrystallization. The authors propose that the lower concentration of dust particles enhance migration recrystallization, leading to smaller $\Delta\varepsilon$ values. This suggests that, at greater depths, the deformation history in the impurity-rich layers is preserved, whereas that in the impurity-poor layers is updated (i.e., lost) by the active migration recrystallization. Additionally, as shown in a positive correlation in impurity-poor layers, even small amounts of dust particles and small variations in their concentration can significantly influence the crystal orientation fabric.

Another feature of the impurity-rich layers was consistently small grain sizes, an effect otherwise referred to as steady state grain size (e.g., Steinbach et al., 2017). This effect is thought to occur in the case that normal grain growth counteracts rotation recrystallization regardless of the initial grain size (Jacka and Li, 1994). The authors propose that the steady grain sizes in the impurity-rich layers appeared at greater depths. At shallower depths, the grain sizes would have been inversely correlated with the dust concentration.

~~**5.5 Variations in the *a*-axis fabric**~~

~~Grain nucleation will also lead to significant changes in *a* axis fabric. However, Because of the lack of data on concerning *a* axes distributions in the depths above 2400 m, UP80% section, we cannot determine the presence or absence of anisotropic *a* axes organizations in this upper section of the dome could not be ascertained. Even so, some. Our observations arewere made, as follows. (i) Firstly, In at many depths within the LO20%, the girdle plane of the *a* axis exhibits strong exhibited a high degree of inhomogeneity depending on θ (refer to the panels in View 4 panels of Figure 4 and Supplementary Information A Section D). (ii) When the Secondly, in the case that the degree of inhomogeneity of the *a* axis within the girdle was expressed as SD_p, the SD_p tends to be these values were generally larger in impurity poor layers and smaller in impurity rich layers (Figure 5). (iii) The Thirdly, the SD_p is well correlated values showed good correlation with grain size, aspect ratio, and $\Delta\varepsilon$ values (Figures 5 and 9). These observations raise several questions.: (i) At Firstly, it would be helpful to know at what depths and how did this *a* axis organization began to form and develop and to understand the underlying mechanism.? (ii) What Secondly, it is unclear if this mechanism involved deformation is the physical mechanism behind this phenomenon – is it deformation, recrystallization, or a combination of both? (iii) What is the spatial scale of the *a* axis organization? Is it limited to the Finally, it remains to be determined if this *a* axis organization was on the size scale of thin sections, or does it extend further?~~

~~Many of tThese questions cannot be conclusively answered solely with the current data alone. However, although speculation is possible During we can speculate based on our significant findings. In dislocation creep, if the slip basal plane is primarily slip plane, the *c* plane (that is, the easy glide plane of hexagonal ice), it is unlikely that *a* axis organization will occur occurs geometrically on this basis. through *c* plane slip. Since these processes (dislocation creep and *a* axis organization) do not seem interdependent, we can exclude this possibility. The organization of the *a* axis structure among the crystal grains can only occur as a result of due to interactions at the grain boundaries between adjacent crystal grains. Therefore,~~

we the authors speculate that dynamic recrystallization processes, particularly migration recrystallization associated with nucleation, play a critical role. The observations listed as (i) to (iii) at the beginning of this section support this speculation.

Unlike migration recrystallization, which can significantly modify *c* axis fabric (e.g., De La Chapelle et al., 1998; Cuffey and Paterson, 2010), rotation recrystallization has a minimal effect on *c* axis fabric changes but does reduce grain size and the aspect ratio. Similarly, it seems reasonable to think that rotation recrystallization has a minimal effect on *a* axis fabric changes as well. Thus, we exclude this as a possible cause of the *a* axis organization. We speculate that It is possible the new grains, with having *c* axis orientations distinctly offset from the single pole cluster will also have new *a* axis orientations. When In the case that these new crystal grains form through via recrystallization, they arrange water molecules will arrange so as to adopt to form the most energetically favourable orientation, minimizing energy between the surfaces of the grains and forming *a* axis alignment This process minimize the energy difference between the surfaces of the grains and produces a axis alignment adjacent grains. Here, we cite two papers by According to Matsuda et al. (1976) and Matsuda and Wakahama (1978), on the possibility of crystal twinning in ice sheets. Crystal twinning occurs when two or more adjacent crystals of the same mineral share some crystal lattice points symmetrically, forming an intergrowth of tightly bonded crystals. The shared surface is known as the twin plane or composition surface. Matsuda et al. (1976) investigated ice core samples from the Antarctic ice sheet near Cape Folger, revealing distinct crystallographic changes at specific depths. The ice layers exhibited a "diamond" pattern in their *c* axis orientations, indicating twinning relationships between crystal groups. The crystal structure of hexagonal ice can have seven directions of oxygen-oxygen bonds, which that are connected by hydrogen bonds, including along the *c* axis. The angles between these bonds are equal to the tetrahedral angle of 109.5°. These authors determined In this prior work, the orientations of all seven oxygen-oxygen bond directions were determined from the orientations of the *c*-axis and *a*-axis orientations ascertained measured in polycrystals with a four-maxima diamond pattern *c*-axis fabric. As a result, it was found that 2 to 3 The data showed that two or three of the seven bonds in each crystal group were aligned with the bond directions of neighbouring crystal groups. This alignment of oxygen-oxygen bond directions between neighbouring crystal groups strongly suggests that the neighbouring crystals might have been in a twinning relationship. Variations in grain size, texture, and crystallographic orientation are linked to deformation under high shear stress, with less deformation and twinning observed in certain layers, leading to characteristic *c*-axis patterns. Matsuda and Wakahama (1978) further investigated several types of polycrystalline ice of different origins. They suggested that a great majority of the adjoining crystals might have been in a twinning relation. They suggested a strong possibility and that the structural relationships between these crystals greatly affects plays a major role in the appearance and growth of nuclei which have having specific orientations during recrystallization.

These findings offer insights into the structural evolution of deep ice in response to stress and impurities; This crystal twinning hypothesis by these authors may apply to the current case of DF study. Although we did not observe a four-maxima *c*-axis pattern was not observed at the DF site, crystal twinning likely occured during nucleation and subsequent crystal growth, leading to shared *a*-axis orientations between adjacent grains, This would occur even before the four-maxima pattern was fully generated. is concretely shaped.

Based on these speculations, we this speculation, the authors propose some answers to the questions posed earlier: (i) This Firstly, *a*-axis organization likely began to appeared and grow increased during periods of enhanced nucleation and migration recrystallization, particularly under at higher temperatures in the LO20%. In the UP80%, this phenomenon is likely very weak. (ii) The most fundamental cause of Secondly, *a* axis rearrangement was evidently caused primarily by nucleation and migration recrystallization, which relieved localized stresses. It is possible that crystal twinning, whereby some crystal lattice points were shared symmetrically, forms produced *a*-axis organization as a means of reaching the most thermodynamically to create the most stable thermodynamic conditions. (iii) The Finally, the spatial extent of *a*-axis rearrangement is thought to be have been relatively limited and likely confined to a small regions, such as the size of a single thin section or even smaller. This conclusion is based on the difficulty in considering because it is difficult to consider a far-reaching effect whereby distant crystal grains align with one each other in terms of the *a* axis. While the *a* axes tend to align among adjacent and nearby crystal

grains, it is natural to consider assume that the orientations formed in coordination become entirely different as the distance increases.

It is also noteworthy that a few several deformation experiments with polycrystalline ice conducted in the laboratory have reported demonstrated *a* axis organization (Journaux et al., 2019; Qi et al., 2019; Wang et al., 2024). These experiments were conducted at temperatures near the melting point of ice, with strain rates much higher (by about approximately 10^5 to 10^7 times) than those in plateau region of the Antarctic ice sheet. A preferred *a* axis maximum was detected in all these shear experiments. Additionally, natural naturally occurring examples of sheared ice at temperatures close to the melting point (Monz et al., 2021; Thomas et al., 2021) have also exhibited a preferred *a* axis maximum. These observations can be explained by based on the same process by which a axis organization result from speculation that the *a* axis organizations were formed due to grain nucleation and migration recrystallization induced by shear strain at temperatures close to the melting point.

5.2 Development of the overall layered structures

5.2.1 Depth-dependent variations of Δ*c* in the entire core

Figure 9 shows Δc, its SD, and the aspect ratio across the entire core thickness. In the UP80%, both Δc and the aspect ratio increase with depth, reaching their maximum levels at the bottom. Below this, between approximately 2400 and 2650 m, the trend changes, with both Δc and the aspect ratio showing larger fluctuations and sharp drops. The decrease in Δc values and the increase in SD are directly linked to the scatter in individual Δc measurements (represented by dots). Pronounced scatter results in smaller averaged Δc values over each 0.5 m segment and larger SD, with a corresponding decrease in the aspect ratio. At depths greater than about 2800 m, Δc values exhibit significant fluctuations over distances of about 10 m, and the aspect ratio remains at its smallest level.

5.2.2 Comparison of *c*-axis fabric at deeper part of three summit ice cores

We extend our comparison of *c*-axis fabric data from DF with that of EDC. It is notable that these two sites are similar in terms of glaciological conditions, including surface temperature, annual mean surface mass balance and ice thickness (see Table 2). Figure 10a indicates the relationship between Δ*c* (averages and raw data as with Figures 5a) value and normalized eigenvalue $a_3^{(2)}$. General trends in cluster strength and grain size are very similar in both ice cores across all age scales. Furthermore, Durand et al. (2009) pointed out depth-dependent developments in *c*-axis clustering in deep sections are similar in the GRIP ice core (Thorsteinsson et al., 1997) and EDC core in Antarctica. Indeed, at the three summit sites, the depth zones where the maximum clustering appears are similar (see Table 2). The similarity among these three sites across both hemispheres implies that certain physical mechanisms are driving this similar development of *c* axis clustering. We hypothesize that the temperature environment within the ice sheet, through mechanisms such as dislocation creep and recrystallization, might have resulted in the commonality of *c* axis fabric at three points in the ice sheets. In this hypothesis, at the bottom of the UP80%, the thickness of ice is approximately 10% of the original ice equivalent thickness at the time of deposition (see Figure 5g). At this depth, the eigenvalue $a_3^{(2)}$ reaches about 0.93. In the absence (or faint presence) of shear stress, a strongly clustered texture will be difficult, either to compress or shear, thereby necessitating dynamic recrystallization as an accommodation process. This state of saturation of the *c*-axis cluster, along with the common temperature range may be more effective as a condition to trigger nucleation and recrystallization. The deepest 10–20% of the polar ice sheets are typically characterized by their ability to easily deform under horizontal shear, due to high temperatures and well-clustered *c*-axis fabric. In these depths, dynamic recrystallization plays a critical role, particularly in impurity-poor layers, to recover the potential of *c*-axis orientations available for the continuation of dislocation-creep-based deformation.

In the present study including Saruya et al. (2022b), we did not identify large anomalous step of *c*-axes clustering with increasing depth (Figures 9, 10 and Supplementary Information D). Rather, *c*-axis fabric exhibits fluctuations that appear

already at a few hundred meter depth at Termination I. Thus, there is no indication attributable to presence of simple shear. This argument differs with the existing scientific claim given by Durand et al. (2007). They suggested the impact of shear was important to explain anomalous strengthening the *c* axes cluster especially at the Termination II. In contrast to this earlier attribution to shear, Saruya et al. (2022b) attribute small depressions of Δc values at MIS5e to the very low concentration of resolved Cl^- ions, which can substitute for the location of H_2O in the crystal lattice, indicating that ice is harder because of it. This explanation applies to the EDC case because, at EDC, most Cl^- ions are lost to the atmosphere from snow compared to DF at least during the Holocene (i.e., the interglacial period), while at Dome Fuji, they are preserved as NaCl and in solid solution (Oyabu et al., 2020). These conditions suggest that ice becomes harder, preventing the *c* axis cluster from strengthening at MIS5e as well. In other words, this gives an alternative explanation for the significant depression of the *c* axis cluster at MIS5e and a notable jump in the *c* axis cluster at EDC. Additionally, further complexity arises because, at EDC, the surface mass balance (SMB) contrast between glacial and interglacial periods is approximately 20% larger than that of DF (Fujita et al., 2015; Parrenin et al., 2016), which will dilute Cl^- ions more at EDC and also complicate ice flow models.

5.3 An overview of the layered structure of the ice sheet

Based on the above discussions, we propose an overview of the layered structure of ice sheets. Polar ice sheets are massive bodies of ice, comprising layers with a wide variety of rheological characteristics, which are dependent on depositional features, that is, historical depositions of aerosols from the atmosphere. The thickness of layers ranges widely, from annual layers (millimeters) to those spanning glacial and interglacial periods. The initial ice fabric forms during firn processes (e.g., Calonne et al., 2017; Fujita et al., 2009, 2016; Montagnat et al., 2020). Another fundamental factor, not covered in the current paper, is the content of ions that either enhance (Cl^- and F^-) or impede (NH_4^+) deformation (Nakamura and Jones, 1970; Jones and Glen, 1969; Jones, 1967), as well as the presence of insoluble particles like salt inclusions, in addition to the dust particles discussed in this study. In ice physics, F^- and NH_4^+ are well-known as major factors that modify the viscosity of ice crystals (as reviewed in textbooks by Petrenko and Whitworth (1999) and Fletcher (1970)). It must be emphasized that these ions can substitute for the location of H_2O in the crystal lattice, thereby modulating the density and behavior of dislocations. These effects from ions are present in the ice crystal lattice from the firn process all the way to the bottom of the ice sheet. For example, Fujita et al. (2014) and Fujita et al. (2016) suggested that the rheology of polar firn is dependent on these ions. Additionally, it must be emphasized that salt inclusions have larger volume fractions than dust particles (Ohno et al., 2005).

Ice with these diverse initial properties, which will persist in the ice, experiences two distinct conditions in the upper 80% and the lower 20% of the ice sheet, as listed in Table 3. Four types of conditions affect the development of crystal orientation fabric, microstructures, and deformational regimes. These are: (i) temperature conditions, (ii) primary strain configurations, (iii) effects of insoluble particles (such as dust, metals, and salts) on texture, and (iv) processes of dynamic recrystallization, including the formation of new grains and migration recrystallization. Consequently, each individual layer has its own trajectory of deformational history over time periods spanning up to 10^6 years.

This overview has significant implications for practical applications, such as ice sheet modelling, ice core sciences and radioglaciology. Practical application for the ice sheet modelling is beyond the scope of this paper. However, these layered structures correlate directly with the vertical thinning of each layer, making them useful for improving ice core dating models by providing constraints on strain values. Additionally, at locations moving away from the dome, the increase in gravity-driven shear movement of the ice sheet causes inhomogeneous deformation between layers or layer zones, eventually resulting in the formation of folds, faults, and mixing of ice across various layer thickness scales. For ice core sciences, which aim to investigate continuous records of very ancient ice on the million-year scale, choosing a drilling site at the dome is crucial. Drilling at locations away from the dome area carries serious risks of layer disturbances near the bottom. Another implication of this discussion concerns the state of radio echoes from the very deep parts, specifically in the lower 20% of the ice sheet. In glaciology, the presence or absence of echo-free zones is a topic of debate (e.g., Fujita et al., 1999; Drews et al., 2009). On

~~one hand, layers of ice *c*-axis fabric can cause the reflection of detectable radio echoes (e.g., Fujita et al., 2000). On the other hand, phenomena in the lower 20% will change the nature of ice for radio wave scattering. Concretely, reflections are more likely from large-scale layers corresponding to glacial/interglacial changes rather than shorter time-scale events. Additionally, layer disturbances accompanied with dynamic recrystallization may be observed as echo-free zones.~~

6 Conclusions

~~***Use of the innovative methods for analysis of crystalline textures, and their outcome***~~

~~For enhanced~~ With the aim of obtaining a better understanding of the layer structures and deformation regimes in the deep sections of polar ice sheets, ~~we~~ this work investigated the lowermost 20% of the DF ice core using innovative analytical methods. ~~Using~~ Based on the Laue X-ray diffraction method, ~~we clarified~~ detailed information was obtained concerning the ~~about both~~ *c*- and *a*-axes ~~for each~~ of individual crystal grain while microstructural~~. Microstructural~~ observations were used to assess ~~provided signals~~ ~~signs of~~ migration recrystallization and potentially nucleated grains. ~~With the~~ The DTM, applied to acquire~~ we provided~~ *c*-axis fabric data with ~~unprecedented~~ high sampling frequency, spatial resolution, and continuity, revealed large and small variations of the *c*-axis cluster strength and the controlling factors of them~~, and statistical significance~~. ~~Furthermore, by~~ By combining the data from these ~~two~~ methods allowed the~~, we clarified the layering of~~ crystal orientation fabric layering to be elucidated. ~~in the LO20%. Coupled with previously reported *c*-axis fabric data in the UP80%, we obtained comprehensive and high-resolution *c*-axis fabric profiles for the core. The complex sequence includes changes in depth range from the UP80% to the LO20%, and temperature variations from about −55℃ to the pressure melting point.~~ The primary strain configurations in the ice were found to transition ~~evolve~~ from vertical compression to a combination of vertical compression and simple shear. Insoluble particles ~~like~~ such as dust were determined to affect this ~~influence the~~ process by shifting from promoting the slower formation of *c*-axis clustering to inhibiting its relaxation of the *c*-axis. ~~Moreover, the~~ The activity of dynamic recrystallization was also determined to increase ~~increases~~ from less active to more active states. ~~Including these, our major conclusions for each specific point are further listed as follows:~~ The primary conclusions obtained from this work are as follows.

~~***Development of crystal orientation fabric, microstructure, and layering***~~

(i) **Development of the *c*-axis clustering and layered structures:** The clustering strength of the single-pole *c*-axis fabric reached a maximum between 2400 and 2640 m. The fluctuations in cluster strength increased substantially below this depth. Up to a depth of 2700 m, the angles of inclination of the *c*-axes cluster and visible layers were approximately consistent but deviated from the vertical. The system rotated as a rigid body as a result of simple shear, while the *c*-axes cluster alone rotated backward because of the compression components of the simple shear applied to the ice. The primary role of shear stress in the deep sections was similar to the effects observed in the EDML ice core (Weikusat et al., 2017).

(ii) **The similarity between the DF and EDC ice cores:** The general trends exhibited by the *c*-axis cluster strength and grain sizes in the present work were approximately the same as those seen in the EDC ice core (Durand et al. 2009). These similarities may be attributed to equivalent impurity concentration profiles (which in turn are associated with climate change) and temperature profiles. Hence, it appears that rigid body rotation does not affect cluster strength.

(iii) **The preferred *a*-axis fabric:** ~~In the LO20%,~~ *a*-axis fabric exhibited preferred orientation within the plane of the *a*-axis girdle, in a spatial scale of the thin sections used for the Laue measurements. Organization of the preferred *a*-axis fabric is enhanced in impurity-poor ice. Additionally, the enhancement of the preferred *a*-axis fabric is well correlated with grain growth.

(iv) **Roles of the nucleation and the migration recrystallization~~, and the crystal twinning~~:** Signals of migration recrystallization, such as bulged grain boundaries and interlocking grains, and potentially nucleated grains were found

in impurity-poor layers. ~~Crystal grains in impurity rich layers showed a flattened (elongated in 2D) shape.~~ These contrasts in microstructures are unique to deeper sections. We argue that the nucleation and the migration recrystallization is the exact physical mechanism that caused the *c*-axis relaxation and the *a*-axis organization. ~~Possibly, crystal twinning, which share some crystal lattice points symmetrically with the neighboring crystals, is forming the *a*-axis organization.~~

(v) **Contrast between impurity rich and impurity poor layers:** ~~**Growth of the *c*-axis clustering, aspect ratio, and grain size** In the LO20%, More impurity rich layers~~ The relationship between cluster strength and the concentration of dusty impurities was found to change at approximately 2640 m. Below this depth, layers having higher concentrations of impurities were found to maintain stronger *c*-axis clustering~~, larger aspect ratios,~~ and smaller grain sizes. In contrast, impurity-poor layers exhibited relaxation of the *c*-axis clustering~~, decreases in the aspect ratios,~~ and increased ~~growth~~ of grain sizes ~~occur~~ due to nucleation and migration recrystallization. These effects modified ~~altering~~ both the *c*-axis and *a*-axis fabric of ~~impurity-poor~~ such layers.

(vi) **Grain size in the deepest sections:** Small grain sizes are maintained between 2900 and 2950 m. Grain boundary pinning by insoluble impurities remains significantly effective even at high temperature close to the melting point. In contrast, below 2960 m, the grain size becomes extremely large. In high temperature environment near the bedrock, small changes in impurity concentration drastically change the microstructures.

~~(vii) **Presence of nucleation in the impurity rich layers:** In impurity rich layers, features indicating nucleation were observed. However, only weak signals of migration recrystallization were observed. The contrasting microstructures between impurity-rich and impurity-poor layers are closely linked to the differing variations in cluster strength in each layer.~~

~~(viii) **Growth of the rigid body rotation:**~~

~~(ix) **Presence of transitions:** Both the clustering strength of *c* axes and the aspect ratio of grains reached a maximum level at the bottom of the UP80% and fluctuated in the LO 20%.~~

~~(x) **The *c*-axis clustering fluctuation over short distances:** In the LO20%, the SD of the clustering strength within many 0.5-m ice segments is much larger than in the UP80%, indicating that the *c*-axis clustering fluctuation over short distances is enhanced in deeper sections.~~

~~***Common and unique features of sites: implications for wider areas in polar ice sheets***~~

~~(i) **Atmospheric aerosols primarily determine ice fabric fluctuations:** The fluctuations of the cluster strength versus ice age are common at DF and EDC, suggesting that depositional features from atmospheric aerosols primarily determine these fluctuations. This suggests that *c*-axis fabric layering is essentially common across a wide area of polar ice sheets, if the deposition of chemical ions and dust is similar among sites.~~

(ii) ~~**The similarity among three dome summit sites:** At the three summit sites in Antarctica (DF and EDC) and Greenland (GRIP), the depth zones where the maximum clustering appears are similar. The similarity among these three sites across both hemispheres may be related to commonality of temperature condition along with the total amount of strain in the LO20%.~~

(iii) **Unusual thickening of annual layers near the base of the DF ice core:** Unusual thickening of annual layers near the base of the DF ice core can be explained by the rigid body rotation of the system in the meridional direction near the bed of the ice sheet.

~~(iv) **An alternative explanation for the depression of the *c*-axis cluster at MIS5c in EDC ice:** The significant reduction of the *c*-axis cluster at MIS5c in EDC is explained by the very low concentration of Cl^- ions in the ice during this period and at this location.~~

(v) **Implications for the nature of the very deep ice:** We argue that the bottom thickness of the ice sheet deeper than approximately 2600 m plays a special role in shear deformation when the ice sheet moves away from the dome. Uneven strains between the layers will eventually compromise the integrity of the ice body in each part of the ice sheets. Consequently, folding, mixing, and faulting lead to the destruction of resolvable continuity in ice core signals. Ice core drilling, aiming the ancient climatic records, at locations away from the dome area carries serious risks of layer disturbances near the bottom. Echo free zones for radar sounding can be explainable as zones with layer disturbances accompanied with enhanced dynamic recrystallization.

These numerous findings warrant further examination for a better understanding. The new data and insights should link directly to key processes governing the flow of polar ice sheets. Expanding the knowledge from the dome summit to a three-dimensional dynamic layer structure within the ice sheet is a critical challenge. Deciphering radar sounding data in depth is key to this endeavor. The internal deformation of the ice sheet modulates flow based on crystal orientation fabric, ion concentration, and micropartiele presence, leading to differential ice movement or disturbances like folds and mixing at various layer thickness scales. These factors can introduce positive or negative feedback, modulating the flow characteristics of the ice sheet.

Data availability

The data used in this paper will be published in the National Institute of Polar Research ADS data repository in conjunction with the publication of the present manuscript in The Cryosphere.

Author contributions

Author contributions are listed herein using the CrediT system (Ghan et al., 2016) to provide greater clarity concerning these contributions of all authors. TS: Conceptualization, Methodology, Validation, Formal analysis, Investigation, Data curation, Writing - Original draft, Visualization. AM: Conceptualization, Methodology, Validation, Formal analysis, Investigation, Data curation, Writing - Review & editing, Visualization. SF: Conceptualization, Methodology, Validation, Formal analysis, Investigation, Writing - Original draft, Supervision, Project administration, Funding acquisition. TK: Investigation, Writing - Review & editing. MI: Investigation. KG-A, MH, AH, YI, HO, WS, and ST: Writing - Review & editing.

Competing interests

The authors declare that they have no conflict of interests.

Acknowledgements

The authors are grateful to all the Dome Fuji Deep Ice Core Project Members who contributed to obtaining the ice core samples, either through logistics, drilling, or core processing. The main logistics support was provided by the Japanese Antarctic Research Expedition (JARE), managed by the Ministry of Education, Culture, Sports, Science and Technology (MEXT). This work was supported by JSPS KAKENHI Grant Number 18H05294.

Appendix A: Microstructures ~~in the deep sections of DF ice core~~: Results and interpretations

A1 Microstructural features in glacial and interglacial periods

The present study~~, we provide~~ provides limited but significant examples of noteworthy microstructures, as shown in Figures A1 and A2. In Figure ~~A2~~, five examples are provided that include impurity-rich ice (panel a: 2648 m, ~270 ppbv dust concentration; panel c: 2759 m, ~137 ppbv), impurity-poor ice (panel b: 2685 m, ~10 ppbv; panel d: 2872 m, ~3 ppbv), and impurity-rich deep ice (panel e: 2909 m, ~80 ppbv). ~~Here, we use the term impurity-rich to mean that ice contains either insoluble particles (like dust) and/or soluble impurities such as dissolved ionic species. The concentration of impurity poor ice is distinctly lower than that of impurity rich ice; the difference is significant. We provide images~~ Images are presented of ice thin sections viewed through crossed polaroids together with *c*-axis fabric data for each grain obtained using the G50 instrument, and microscopy images. The thin black lines in the microscopy images indicate grain boundaries. Such boundaries on the reverse side of a thin section ~~are visible~~ appear as thinner lines. Illustrates of the front and reverse side grain boundaries~~, grain boundaries on the reverse side,~~ and the subgrain boundaries are provided in Figure S3 in Supplementary Information Section 1.5. ~~The legend for *c* axis fabric data is given as a circle at the bottom of Figure 6. The color of each grain indicates *c* axis orientation; the red color means that the *c* axis has an orientation in the vertical. As for the *c* axis orientation, at panels (a) and (c),~~ Panels (a) and (c) show numerous ~~we observe many~~ small grains with *c*-axis orientations ~~distinctly~~ that are obviously offset from the vertical direction (see the *c*-axis fabric image). These grains are sparsely distributed,~~The size of such small grains range in the order of a millimeter or much less. Additionally, we observe that flattened (or, elongated in 2D) shape of grans that is slanting.~~ And typically have sizes on the order of a millimetre or less. Flattened (or two-dimensionally elongated) grains having a noticeable slant are also evident. These features were ~~unique~~ present in the impurity-rich depths but absent at impurity-poor depths. In the case of (b) and (d), we observe much coarser grains are apparent with a *c*-axis orientation distinctly offset from the vertical direction. Compared with the results for ~~to the cases of~~ the impurity-rich layers, these coarser grains occupy much larger areas in the image, having diameters of a several millimets. In the case of the two deepest samples (panels (d) and (e)), it is evident that the crystal grain boundaries ~~tend to be distributed as more straight lines~~ are often appear as straight lines~~, and there are~~ with few subgrain boundaries. Panel (e) shown as an ~~is a sample of~~ impurity-rich layers, in which the crystal grains are coarse relative to those in~~; crystal grain is coarser compared to~~ (a) and (c). However, some characteristics of the impurity-rich layers observed in panels (a) and (c) are less pronounced ~~persistently present~~ in (e). ~~That is, flattened grains have slanting features. Additionally, grains with *c* axis orientations distinctly offset from the vertical direction occupy only a small area within the image.~~

The $\Delta\varepsilon$ values were affected by the volume fraction of grains having a *c*-axis orientation that was significantly offset from the surrounding grains. ~~As for the link between ice fabric eigenvalues and the microstructure, $\Delta\varepsilon$ values are significantly affected by volume fraction of grains with *c*-axis orientation distinctly offset from surrounding grains. Coarser grain is more influential compared to sparsely distributed smaller grains. An example of comparison them is provided in Supplementary Information C. Because the $\Delta\varepsilon$ values are volume weighted averages within the microwave beam, $\Delta\varepsilon$ values decreases more when there are more grains (in size and number) with *c* axis orientation distinctly offset from surrounding grains.~~ In this regard, the coarser grains also had a greater effect compared with the more sparsely distributed smaller grains. Because the $\Delta\varepsilon$ values represented volume-weighted averages within the microwave beam, these values were decreased to a greater extent in the case that more and/or larger grains with *c*-axis orientations distinctly offset from the surrounding grains were present.

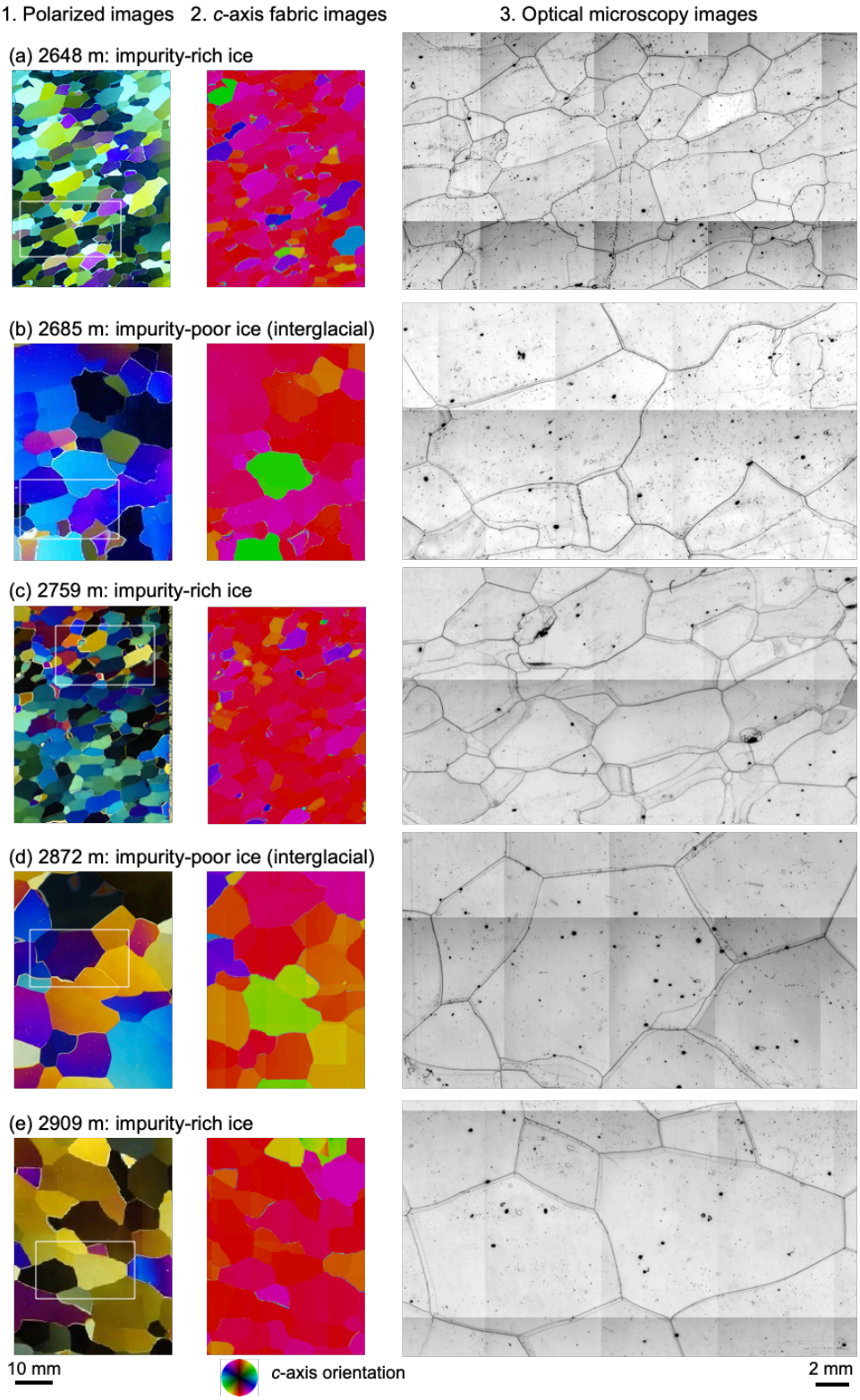

Figure A1 Microstructure images ~~representing examples~~ of typical specimens from five depths. The depths and types for each specimen are specified in the figure. For each depth, an image of a thin section viewed through crossed polaroids (left), a *c*-axis fabric image (centre) and optical microscopy images (right) are presented. In the optical microscopy images, thin black lines indicate grain boundaries while grain~~.~~ ~~Grain~~ boundaries on the reverse side of ~~a thin section~~ the sample are visible as thinner lines. ~~White frames~~ The white rectangles in the leftmost column indicate the locations from which for microscopy images shown in the right column were obtained. A legend concerning the colour coding of the c-axis orientation data in the ~~For the *c*-axis fabric~~ images in the central column is provided~~, the legend for *c*-axis orientation is given~~ at the base of the figure ~~bottom~~: The colour of each grain indicates the orientation of the *c*-axis~~. Red~~ with red showing a~~color means that *c*-axis has the~~ vertical orientation.

A2 Microstructures in the impurity-rich layer: grain elongation and smaller grain sizes

~~It is remarkable that~~ Remarkably, the crystal grains in the impurity-rich layers ~~tend to be~~ were often flattened and the major axes of these grains were inclined ~~incline~~ away from the horizontal directions. These features were not identified in the ~~seem absent in~~ surrounding impurity-poor (interglacial) layers. An example of the slanting and flattened grains is shown in Figure A2a. To better assess this ~~As for the~~ grain flattening, ~~we analyzed~~ the aspect ratio based on the ~~short and long~~ long and short axes of a two-dimensional fitted ellipse ~~in 2D~~ using the ImageJ software. These aspect ratios were found to differ significantly ~~distinctly different~~ between in the impurity-rich layer and in the impurity-poor layers, with values in the ranges of ~~. In the impurity rich layers it ranged~~ 1.9–2.0~~, while in impurity poor layers it was smaller,~~ and 1.5–1.7, respectively. More detailed data ~~in the LO20%~~ are provided in Table S4 in Supplementary Information Section A5. ~~They are displayed in Figure 9 along with the aspect ratio reported from the UP80% of the DF1 ice core (Azuma et al.1999, 2000). We observe that in the UP80%, the aspect ratio increased steadily, while in the LO20%, the aspect ratio tended to decrease, showing a clear distinction between higher values of impurity rich layers and lower values of impurity poor layers. Transition from the increasing trend to the decreasing trend is at depths approximately 2500 m (Figure 9). These features of the transition are very similar to the case of the grain size, noted in section 4.4. Azuma et al. (1999) suggested that nucleation recrystallization is not active above 2500 m depth and that deformation and rotation recrystallization affect the increasing trend of grain size and thus aspect ratio. However, below the transition at ~ 2500 m, situations are different in terms of nucleation recrystallization, which we will discuss later in this paper.~~

~~Regarding the flattened features within the impurity rich layers, Azuma et al. (1999, 2000) demonstrated growth of flattening of the grains in the UP80%, which is the basis of the aspect ratio shown in Figure 9.~~ A similar two-dimensional feature, known as the "brick-wall pattern", has been reported to occur in layers having high concentration of impurities from ~~at the high-impurity ice layers of~~ the Antarctic EDML ice core (Faria, 2009) but this phenomenon has not yet been observed ~~it has not been reported in~~ the Antarctic EDC ice core. ~~For the Greenland NEEM ice core,~~ Kuiper et al. (2020) found ~~that~~ fine-grained bands with flattened (or elongated in two dimensions) grains ~~with~~ having an aspect ratio of 2 in the Greenland NEEM ice core.~~, which is as large as the maximum level in the DF core.~~ This aspect ratio was as large as the maximum value observed in the DF core specimens. ~~For the EDML core,~~ Weikusat et al. (2017) suggested that shear deformation was responsible for the flattened (or, elongated) grains identified in the EDML core, while Faria et al. (2009) proposed that deformation via microscopic grain boundary sliding via microshear ~~was a deformation mechanism for making~~ generated the brick-wall pattern. According to these prior studies, ~~authors, a condition favorable for the occurrence of~~ grain boundary sliding is likely promoted by a combination of smaller grain sizes, the presence of moderate stress, and higher temperatures. Smaller grain sizes often occur in ~~achieved by~~ the presence of high impurity concentrations of impurities and these~~. These~~ conditions are typically found in the impurity-rich layers in the deeper sections of ice sheets (Faria et al. 2009). ~~On the one hand, in the LO20%~~, Grain elongation becomes less pronounced in more deeper sections, as shown in Figure A1e, which provide data for a sample from a depth of 2909 m.~~ (sample from a depth 2909 m) and Figure 9~~. ~~We~~ The authors suggest that the flattened features were maintained ~~remain,~~but were reduced they are weakened by recovery and recrystallization processes occurring at high temperatures ~~due to exposure of ice to high temperature~~ close to melting point of the ice ~~for time periods in the order of 10^5 years~~. The extent of flattening could be determined by the temperature of the ice, and thus the depth, and by the mpurity concentration. ~~Strength of the flattened feature is~~~~could be~~ ~~dependent on temperature (thus, depth) and impurity concentration.~~

Another feature of the impurity-rich layers was ~~persistently~~ consistently small grain sizes (Figure 5e), and effect otherwise referred to ~~Such a feature is observed in MIS10, 12, 14 and 16, where the concentration of dust particles is extremely high. The small size is clearly deviated from the growth trend in the UP80% (Figure 10e). This persistently small grain size in ice core is known~~ as "steady state grain size" (e.g., Steinbach et al., 2017). ~~It is believed that steady state grain size is achieved when~~ This effect is thought to occur in the case normal grain growth counteracts rotation recrystallization regardless of the initial grain size (Jacka and Li, 1994). ~~We suggest~~ The authors propose that the steady grain sizes in the impurity-rich layers

appeared at greater depths. ~~established themselves after these layers had reached deeper depths.~~ ~~When the impurity-rich layers were~~ At shallower depths ~~in the past,~~ the grain sizes would have been inversely correlated with the dust concentration.

A3 Migration recrystallization and grain nucleation

In dynamic recrystallization processes, rotation recrystallization has a minimal effect on the *c*-axis fabric changes but reduces both the grain size and the aspect ratio. In contrast, migration recrystallization can significantly modify the *c*-axis fabric (e.g., De La Chapelle et al., 1998; Cuffey and Paterson, 2010). In the case that several neighbouring grains contain different amounts of ~~When a difference in~~ stored strain energy ~~exists between a few neighboring grains~~, the grain boundary will migrate~~s~~ towards the higher-energy grain (e.g. Faria et al., 2014b). During this strain-induced migration recrystallization, grain boundaries sometimes become irregular~~, forming~~ and form interlocking patterns (Duval and Castelnau, 1995; Faria et al., 2014b). Figures A2b and A2c show a specimen ~~examples~~ from a depth of 2685 m with features presumably resulting from ~~formed by~~ strain-induced migration recrystallization. In panel (b), the ~~top-left~~ large grain in the upper left (b1) ~~has~~ exhibits a convex grain boundary ~~toward~~ with the adjacent grain (b2) whereas in~~. In~~ panel (c), the lower ~~bottom~~ grain (c1) has a convex grain boundary ~~toward~~ with the adjacent grain (c3). The presence of numerous subgrain boundaries implies a region of high strain that is heterogeneously dispersed ~~highly and heterogeneously strained region~~ (Faria et al., 2014b; Stoll et al., 2021a). Interlocking grains are ~~shown~~ evident in Figure A2d, which presents images for a ~~(~~sample from a depth of 2872 m~~)~~. Here grains ~~Grains with~~ having various *c*-axis orientations are intricately interwoven (see the *c*-axis fabric image). It should also be noted that these ~~These~~ features were evident in impurity-poor layers. ~~Contrastingly,~~ ~~Conversely, in impurity-rich ice, grains with *c*-axis orientations and distinctly offset from the vertical in impurity-rich ice were~~are present as smaller grains ~~and surrounded by larger grains (Figures A1a, A1c and A2a).~~

~~It is believed that grain nucleation occurs at triple junctions,~~ Grain nucleation in ice is thought to occur at grain boundaries ~~and as two-sided grains,~~ or similar regions characterized by high concentration of dislocation walls and subgrain boundaries (Faria et al. 2014b). ~~We~~ The authors note that it is very challenging to identify a grain immediately following nucleation ~~identification for a "just nucleated grain" is very difficult~~, as this requires a series of observations over time.The time ~~time-series observations. Rather, when nucleation occurs, it~~ may grow immediately after nucleation in natural ice samples and so observation can be difficult. However, considering the morphological features of the small grains with a *c*-axis distinctly offset from that of surrounding ~~surrounded by~~ larger grains (Figures A1a, A1c and A2a), ~~we suggest that these may be grains that these grains may have been~~ nucleated at some ~~timing of~~ point during the deformational history of the ice within the ice sheet.

Although there have been several studies investigating grain nucleation in artificially deformed ice (e.g., Montagnat et al., 2015; Chauve et al., 2017), there have been few reports of this process in ~~are not enough examples with~~ natural ice samples. Faria et al. (2014b) suggested that a nucleated grain will not exhibit internal structures but will bulge ~~bulges~~ toward a region rich in dislocation walls and subgrain boundaries. Examples of grains with such features are shown in Figures A2e and A2f. Small grains with no internal structures (e1 and f1) can be seen to be situated ~~are located~~ at grain boundaries. ~~In case of these grains (e1 and f1), they~~ These grains have *c*-axis orientations close to those of the adjacent grains (e2 and f2) (see the *c*-axis fabric images in panels e and f). ~~Nucleation of grains are further discussed in section 5 in this paper.~~

~~As a phenomenon~~ Dust particle segregation was found to be associated with grain boundary migration~~, we observed dust particle segregation~~ (Figure A2g). Note that, in this figure, the thin lines adjacent to the grain boundary represent the reverse side of the grain boundary and indicate that~~. Therefore,~~ dust particles were segregated along the planes of the crystal grains. Grain boundary migration in the deeper parts of the ice core likely ~~leads to~~ promoted the redistribution of soluble impurities and dust particles.

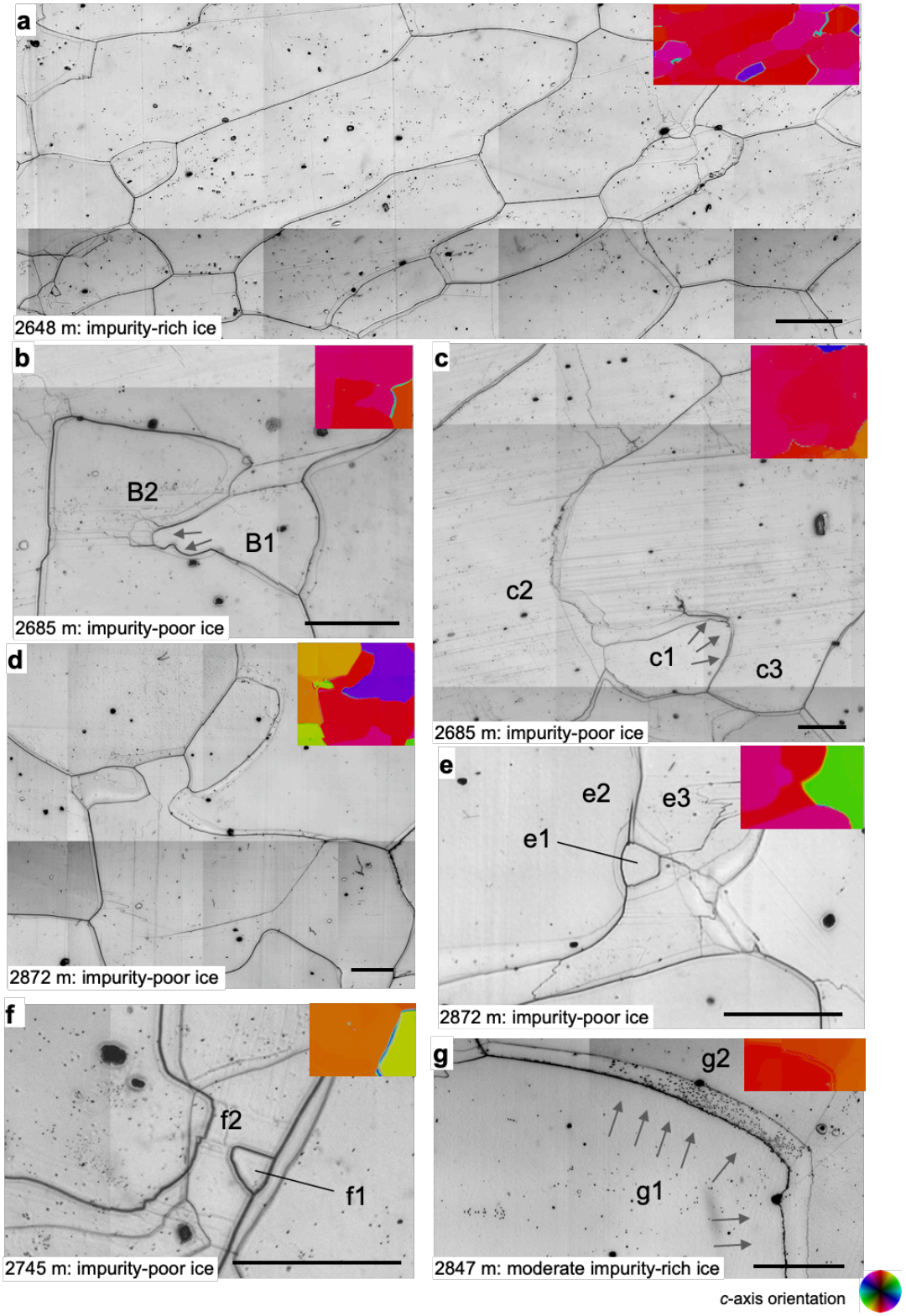

Figure A2. Images of microstructures in specimens from five depths showing ~~Microstructure images illustrating features of~~ grain elongation and migration recrystallization. ~~Images from five selected depths are presented.~~ The depths are indicated in each panel and also summarized at the top of Figure 5. All images were ~~observed using~~ acquired from vertical thin sections. The solid black lines indicate grain boundaries~~.~~ ~~Grain~~ while grain boundaries on the reverse side of each thin section are visible as thin lines. The arrows indicate convex grain boundaries. Colour coding of the *c*-axis fabric image in each panel indicates the *c*-axis orientation of each grain and the accompanying~~. The~~ legend ~~for c-axis fabric images~~ is displayed at the bottom right. Grains shown in red and green/blue have the c-axis oriented vertically and horizontally, respectively. ~~Red-colored grains have a *c*-axis oriented vertically, while green or blue-colored grain are inclined horizontally.~~ (a) Flattened (or elongated in two dimensions) and slanting grains observed in the impurity-rich layer. (b) and (c) Typical results from a depth of 2685 m. (b) The small grain (b1) grain ~~has bulged~~ with bulging (cuspidate) grain boundaries. (c) ~~Bottom~~ The lower grain (c1) ~~has bulged~~ with bulging (cuspidate) grain boundaries. (d) An example of interlocking grains in a sample from a depth of 2872 m. Grains with various *c*-axis orientations are intricately interwoven. (e) and (f) Possible examples of grain nucleation in samples from depths of 2872 and 2745 m. The

small grains (e1 and f1) exhibit a lack of internal structures such as slip bands and subgrain boundaries, while the adjacent grains display many slip bands and subgrain boundaries. ~~The small grains are located at grain boundaries as two-sided grains.~~ (g): The segregation of dust particles along the front of a grain boundary in a sample from a depth of 2847 m. Scale bars: 2mm.

References

Abbasi, R., Ackermann, M., Adams, J., Aggarwal, N., Aguilar, J., Ahlers, M., et al. (2024). In situ estimation of ice crystal properties at the South Pole using LED calibration data from the IceCube Neutrino Observatory. The Cryosphere, 18(1), 75–102. https://tc.copernicus.org/articles/18/75/2024, 2024

Alley, R.B.: Flow law hypotheses for ice sheet modelling, J. Glaciol., 38(12), 245–256, https://doi.org/10.3189/S0022143000003658, 1992.

Alley, R. B., and Woods, G. A.: Impurity influence on normal grain growth in the GISP2 ice core, Greenland, J. Glaciol., 42(141), 255–260, https://doi.org/10.3189/S0022143000004111, 1996.

Azuma, N.: A flow law for anisotropic polycrystalline ice under uniaxial compressive deformation, Cold Reg. Sci. Tech., 23, 137–147, https://doi.org/10.1016/0165-232X(94)00011-L, 1995.

Azuma, N. and Goto-Azuma, K.: An anisotropic flow law for ice-sheet ice and its implications, Ann. Glaciol., 23, 202–208, https://doi.org/10.3189/S0260305500013458, 1996.

Azuma, N., Wang, Y., Mori, K., Narita, H., Hondoh, T., Shoji, H., and Watanabe O.: Textures and fabrics in the Dome F (Antarctica) ice core, Ann. Glaciol., 29, 163–168, https://doi.org/10.3189/172756499781821148, 1999.

Azuma, N., Wang, Y., Yoshida, Y., Narita, H., Hondoh, T., Shoji, H., and Watanabe, O.: Crystallographic analysis of the Dome Fuji ice core, in: Physics of Ice Core Records, edited by: Hondoh, T., Hokkaido University Press, Sapporo, 45–61, 2000.

Bamber, J. L., Gomez-Dans, J. L., and Griggs, J. A.: Antarctic 1 km Digital Elevation Model (DEM) from combined ERS-1 radar and ICESat Laser satellite altimetry, in: National Snow and Ice Data Center, Digital media, Boulder, Colorado, USA, 2009.

Bazin, L., Landais, A., Lemieux-Dudon, B., Toyé Mahamadou Kele, H., Veres, D., Parrenin, F., Martinerie, P., Ritz, C., Capron, E., Lipenkov, V., Loutre, M.F., Raynaud, D., Vinther, B., Svensson, A., Rasmussen, S. O., Severi, M., Blunier, T., Leuenberger, M., Fischer, H., Masson-Delmotte, V., Chappellaz, J., and Wolff, E.: An optimized multi-proxy, multi-site Antarctic ice and gas orbital chronology (AICC2012): 120–800 ka, Clim. Past, 9(4), 1715–1731, https://doi.org/10.5194/cp-9-1715-2013, 2013.

Budd, W. F. and Jacka, T. H.: A Review of Ice Rheology for Ice Sheet Modelling, Cold Reg. Sci. Tech., 16, 107–144, https://doi.org/10.1016/0165-232X(89)90014-1, 1989.

Buizert, C., Fudge, T. J., Roberts, W. H. G., Steig, E. J., Sherriff-Tadano, S., Ritz, C., Lefebvre, E., Edwards, J., Kawamura, K., Oyabu, I., Motoyama, H., Kahle, E. C., Jones, T. R., Abe-Ouchi, A., Obase, T., Martin, C., Corr, H., Severinghaus, J. P., Beaudette, R., Epifanio, J. A., Brook, E. J., Martin, K., Chappellaz, J., Aoki, S., Nakazawa, T., Sowers, T., Alley, R., Ahn, J., Sigl, M., Severi, M., Dunbar, N. W., Svensson, A., Fegyveresi, J., He, C., Liu, Z., Zhu, J., Otto-Bliesner, B., Lipenkov, V., Kageyama, M., and Schwander, J.: Antarctic-wide surface temperature and elevation during the Last Glacial Maximum, Science, 372, 1097–1101, https://doi.org/10.1126/science.abd2897, 2021.

Calonne, N., Montagnat, M., Matzl, M., and Schneebeli M.: The layered evolution of fabric and microstructure of snow at Point Barnola, Central East Antarctica, Earth Planet. Sci. Lett., 460, 293–301, https://doi.org/10.1016/j.epsl.2016.11.041, 2017.

Castelnau, O., Thorsteinsson, T., kipfstuhl, J., Duval, P., and Canova, G. R.: Modelling fabric development along the GRIP ice core, central Greenland, Ann. Glaciol., 23, 194-201, https://doi.org/10.3189/S0260305500013446, 1996.

Castelnau, O., Shoji, H., Mangeney, A., Milsch, H., Duval, P., Miyamoto, A., Kawada, K., and Watanabe, O.: Anisotropic behavior of GRIP ices and flow in Central Greenland, Earth Planet. Sc. Lett., 154, 307-322, https://doi.org/10.1016/S0012-821X(97)00193-3, 1998.

Chauve, T., Montagnat, M., Barou, F., Hidas, K., Tommasi, A., and Mainprice, D.: Investigation of nucleation processes during dynamic recrystallization of ice using cryo-EBSD, Phil. Trans. R. Soc. A, 375, 20150345, http://dx.doi.org/10.1098/rsta.2015.0345, 2017.

Church, J., Clark, P., Cazenave, A., Gregory, J, Jevrejeva, S., Levermann, A., Merrifield, M., Milne, G., Nerem, R., Nunn, P., Payne, A., Pfeffer, W., Stammer, D. and Unnikrishnan, A.: Sea Level Change. In: Climate Change 2013: The Physical Science Basis. Contribution of Working Group I to the Fifth Assessment Report of the Intergovernmental Panel on Climate Change (IPCC), Cambridge University Press, Cambridge, 1137–1216, 2013.

Cuffey, K. M., and Paterson, W. S. B.: The Physics of Glaciers, 4th edition, Elsevier, Amsterdam, 2010.

Cullen, A. L.: Infrared and Millimeter Waves, in Millimeter-Wave Open-Resonator Techniques, Academic Press, New York, pp. 233–280, 1983.

Dahl-Jensen, D., Johnsen, S. J., Hammer, C. U., Clausen, H. B., and Jouzel, J.: Past Accumulation rates derived from observed annual layers in the GRIP ice core from Summit, Central Greenland, In: Peltier, W.R. (eds) Ice in the Climate System. NATO ASI Series, vol 12. Springer, Berlin, Heidelberg. https://doi.org/10.1007/978-3-642-85016-5_29, 1993.

Dahl-Jensen, D., Mosegaard, K., Gundestrup, N., Clow, G. D., Johnsen, S. J., Hansen, A. W., and Balling, N.: Past Temperatures Directly from the Greenland Ice Sheet, Science, 282, 268–271, https://doi.org/10.1126/science.282.5387.268, 1998.

De La Chapelle, S., Castelnau, O., Lipenkov, V., and Duval, P.: Dynamic recrystallization and texture development ice as revealed by the study of deep ice cores Antarctica and Greenland, J. Geophys. Res., 103, 5091–5105, https://doi.org/10.1029/97JB02621, 1998.

Dome Fuji Ice Core Project Members: State dependence of climatic instability over the past 720,000 years from Antarctic ice cores and climate modeling, Sci. Adv., 3(2), e1600446, https://doi.org/10.1126/sciadv.1600446, 2017.

Drews, R., Eisen, O., Weikusat, I., Kipfstuhl, S., Lambrecht, A., Steinhage, D., Wilhelms, F., and Miller, H.: Layer disturbances and the radio-echo free zone in ice sheets, The Cryosphere, 3, 195–203, https://doi.org/10.5194/tc-3-195-2009, 2009.

Durand, G., Weiss, J., Lipenkov, V., Barnola, J., Krinner, G., Parrenin, F., Delmonte, B., Ritz, C., Duval, P., and Röthlisberger, R.: Effect of impurities on grain growth in cold ice sheets, J. Geophys. Res., 111(F1)., F01015, https://doi.org/10.1029/2005JF000320, 2006.

Durand, Gillet-Chaulet, F., Svensson, A., Gagliardini, O., Kipfstuhl, S., Meyssonnier, J., Parrenin, F., Duval, P., and Dahl-Jensen, D.: Change in ice rheology during climate variations - implications for ice flow modelling and dating of the EPICA Dome C core, Clim. Past, 3, 155-167, https://doi.org/10.5194/cp-3-155-2007, 2007.

Durand, G., Svensson, A., Persson, A., Gagliardini, O., Gillet-Chaulet, F., Sjolte, J., Montagnat M., Dahl-Jensen, D.: Evolution of the texture along the EPICA Dome C ice core, in: Physics of Ice Core Records II, edited by: Hondoh, T., Hokkaido University Press, Sapporo, 91–105, 2009.

Duval, P.: Creep and Fabrics of Polycrystalline Ice Under Shear and Compression, J. Glaciol., 27, 129-140, https://doi.org/10.3189/S002214300001128X, 1981.

Duval, P. and Le Gac, H.: Mechanical Behaviour of Antarctic Ice, Ann. Glaciol., 3, 92-95, https://doi.org/10.3189/S0260305500002585, 1982.

Duval, P., Ashby, M. F., and Anderman, I.: Rate-controlling pro- cesses in the creep of polycrystalline ice, J. Phys. Chem., 87, 4066–4074, https://doi.org/10.1021/j100244a014, 1983.

Duval, P. and Castelnau, O.: Dynamic recrystallization of ice in polar ice sheets, J. Phys. III, 5, 197–205, https://doi.org/10.1051/jp4:1995317, 1995.

Eichler, J., Kleitz, I., Bayer-Giraldi, M., Jansen, D., Kipfstuhl, S., Shigeyama, W., Weikusat, C., and Weikusat, I.: Location and distribution of micro-inclusions in the EDML and NEEM ice cores using optical microscopy and in situ Raman spectroscopy, The Cryosphere, 11, 1075-1090, https://doi.org/10.5194/tc-11-1075-2017, 2017.

Eisen, O., Steinhage, D., Karlsson, N. B., Binder, T., Helm, V.: Ice thickness of Dome Fuji region, Antarctica, recorded with the AWI airborne radar system: line 20172048. PANGAEA, https://doi.org/10.1594/PANGAEA.920649, 2020.

EPICA Community Members: Eight glacial cycles from an Antarctic ice core, Nature, 429, 623–628, https://doi.org/10.1038/nature02599, 2004.

Fan, S., Hager, T. F., Prior, D. J., Cross, A. J., Goldsby, D. L., Qi, C., Negrini, M., and Wheeler, J.: Temperature and strain controls on ice deformation mechanisms: insights from the microstructures of samples deformed to progressively higher strains at −10, −20 and −30 °C, The Cryosphere, 14, 3875-3905, https://doi.org/10.5194/tc-14-3875-2020, 2020.

Faria, S. H., Kipfstuhl, S., Azuma, N., Freitag, J., Weikusat., I., Murshed, M. M., and Kuhs, W. F.: The Multiscale Structure of Antarctica Part I: Inland Ice, in: Physics of Ice Core Records II, edited by: Hondoh, T., Hokkaido University Press, Sapporo, 39–59, 2009.

Faria, S. H., Weikusat, I., and Azuma, N.: The microstructure of polar ice. Part I: Highlights from ice core research, J. Struct. Geol., 61, 2–20, http://dx.doi.org/10.1016/j.jsg.2013.09.010, 2014a.

Faria, S. H., Weikusat, I., and Azuma, N.: The microstructure of polar ice. Part II: State of the art, J. Struct. Geol., 61, 21–49, http://dx.doi.org/10.1016/j.jsg.2013.11.003, 2014b.

Fitzpatrick, J. J., Voigt, D. E., Fegyveresi, J. M., Stevens, N. T., Spencer, M. K., Cole-Dai, J., Alley, R. B., Jardine, G. E., Cravens, E. D., Wilen, L. A., Fudge, T. J., and McConnell, J. R.: Physical properties of the WAIS Divide ice core, J. Glaciol., 60, 1181-1198, http://dx.doi.org/10.3189/2014JoG14J100, 2014.

Fletcher, N. H.: The Chemical Physics of Ice, Cambridge University Press, Cambridge, http://dx.doi.org/10.1017/CBO9780511735639, 1970.

Fujita, S., Nakawo, M., and Mae, S.: Orientation of the 700m Mizuho core and its strain history., Proc. NIPR Symp. Polar Meteorol. Glaciol., 1, 122-131, https://doi.org/10.15094/00003530, 1987

Fujita, S., Maeno, H., Uratsuka, S., Furukawa, T., Mae, S., Fujii, Y., and Watanabe, O.: Nature of radio echo layer in the Antarctic ice sheet detected by a two-frequency experiment, J. Geophys. Res., 104(B6), 13013-13024, https://doi.org/10.1029/1999JB900034, 1999.

Fujita, S., Maeno, H., and Matsuoka, K.: Radio-wave depolarization and scattering within ice sheets: a matrix-based model to link radar and ice-core measurements and its application, J. Glaciol., 52, 407-424, https://doi.org/10.3189/172756506781828548, 2006

Fujita, S., Okuyama, J., Hori, A., and Hondoh, T.: Metamorphism of stratified firn at Dome Fuji, Antarctica: A mechanism for local insolation modulation of gas transport conditions during bubble close off, J. Geophys. Res., 114, F03023, https://doi.org/10.1029/2008JF001143, 2009.

Fujita, S., Holmlund, P., Matsuoka, K., Enomoto, H., Fukui, K., Nakazawa, F., Sugiyama, S., and Surdyk, S.: Radar diagnosis of the subglacial conditions in Dronning Maud Land, East Antarctica, The Cryosphere, 6, 1203–1219, https://doi.org/10.5194/tc-6-1203-2012, 2012.

Fujita, S., Hirabayashi, M., Goto-Azuma, K., Dallmayr, R., Satow, K., Zheng, J., and Dahl-Jensen, D.: Densification of layered firn of the ice sheet at NEEM, Greenland, J. Glaciol., 60, 905-921, https://doi.org/10.3189/2014JoG14J006, 2014.

Fujita, S., Parrenin, F., Severi, M., Motoyama, H., and Wolff, E. W.: Volcanic synchronization of Dome Fuji and Dome C Antarctic deep ice cores over the past 216 kyr, Clim. Past, 11, 1395-1416, https://doi.org/10.5194/cp-11-1395-2015, 2015.

Fujita, S., Goto-Azuma, K., Hirabayashi, M., Hori, A., Iizuka, Y., Motizuki, Y., Motoyama H., and Takahashi, K.: Densification of layered firn in the ice sheet at Dome Fuji, Antarctica, J. Glaciol., 62(231), 103–123, https://doi.org/10.1017/jog.2016.16, 2016.

Ghan, S., Crawford, J., Langematz, U., Leung, R., Li, Z., Russell, L., Steiner, A., and Zhang, C.: Author contributions can be clarified, J. Geophys. Res., 121, 8155–8155, https://doi.org/10.1002/2016JD025417, 2016.

Goodman, D. J., Frost, H. J., and Ashby, M. F.: The plasticity of polycrystalline ice, Philos. Mag., 43(3), 665–695, https://doi.org/10.1080/01418618108240401, 1981.

Goto-Azuma, K., Hirabayashi, M., Motoyama, H., Miyake, T., Kuramoto, T., Uemura, R., Igarashi, M., Iizuka, Y., Sakurai, T., and Horikawa, S.: Reduced marine phytoplankton sulphur emissions in the Southern Ocean during the past seven glacials, Nat. Commun., 10(1): 1–7, https://doi.org/10.1038/s41467-019-11128-6, 2019.

Gödert, G. and Hutter, K.: Induced anisotropy in large ice shields: theory and its homogenization, Continuum Mech. Thermodyn., 10, 293–318, https://doi.org/10.1007/s001610050095, 1998.

Goldsby, D. L. and Kohlstedt, D. L.: Superplastic deformation of ice: Experimental observations, J. Geophys. Res., 106, 11017–11030, https://doi.org/10.1029/2000JB900336, 2001.

Gow, A. J. and Williamson, T.: Rheological implications of the internal structure and crystal fabrics of the West Antarctic ice sheet as revealed by deep core drilling at Byrd Station, GSA Bulletin, 87, 1665–1677, https://doi.org/10.1130/0016-7606(1976)87<1665:RIOTIS>2.0.CO;2, 1976.

Hargreaves, N. D.: The radio-frequency birefringence of polar ice, J. Glaciol, 21(85), 301–313, https://doi.org/10.3189/S0022143000033499, 1978.

Higashi, A., Nakawo, M., Narita, H., Fujii, Y., Nishio, F., and Watanabe, O.: Preliminary Results of Analyses of 700 m Ice Cores Retrieved at Mizuho Station, Antarctica, Ann. Glaciol., 10, 52–56, https://doi.org/10.3189/S026030550000416X, 1988.

Humphreys, F. and Hatherly, M.: Recrystallization and Related Annealing Phenomena, 2nd edn., Elsevier, https://doi.org/10.1016/B978-0-08-044164-1.X5000-2, 2004.

Inoue, R., Fujita, S., Kawamura, K., Oyabu, I., Nakazawa, F., Motoyama, H., and Aoki, T.: Spatial distribution of vertical density and microstructure profiles in near-surface firn around Dome Fuji, Antarctica, The Cryosphere, 18, 425–449, https://doi.org/10.5194/tc-18-425-2024, 2024.

Jacka, T. and Li, J.: The steady-state crystal size of deforming ice, Ann. Glaciol., 20, 13–18, https://doi.org/10.3189/1994AoG20-1-13-18, 1994.

Journaux, B., Chauve, T., Montagnat, M., Tommasi, A., Barou, F., Mainprice, D., and Gest, L.: Recrystallization processes, microstructure and crystallographic preferred orientation evolution in polycrystalline ice during high-temperature simple shear, The Cryosphere, 13, 1495–1511, https://doi.org/10.5194/tc-13-1495-2019, 2019.

Johnson, A. F.: Creep characterization of transversely isotropic metallic materials, J. Mech. Phys. Solids, 25, 117–126, https://doi.org/10.1016/0022-5096(77)90007-2, 1977.

Jones, R. G.: The measurement of dielectric anisotropy using a microwave open resonator, J. Phys. D: Applied Physics, 9(5), 819–827, https://doi.org/10.1088/0022-3727/9/5/015, 1976a.

Jones, R. G.: Precise dielectric measurements at 35 GHz using an open microwave resonator, Proc. IEEE, 123(4), 285–290, http://doi.org/10.1049/piee.1976.0067, 1976b.

Jones, S., and Glen, J.: The effect of dissolved impurities on the mechanical properties of ice crystals, Philos. Mag., 19(157), 13–24, https://doi.org/10.1080/14786436908217758, 1969.

Kipfstuhl, S., Faria, S. H., Azuma, N., Freitag, J., Hamann, I., Kaufmann, P., Miller, H., Weiler, K., and Wilhelms, F.: Evidence of dynamic recrystallization in polar firn, J. Geophys. Res., 114, B05204, https://doi.org/10.1029/2008JB005583, 2009.

Komiyama, B., Kiyokawa, M., and Matsui, T.: Open resonator for precision dielectric measurements in the 100 GHz band. IEEE Trans. Microw. Theory Tech., 30(10), 1792–1796, https://doi.org/10.1109/22.88556, 1991.

Kuiper, E.-J. N., Weikusat, I., de Bresser, J. H. P., Jansen, D., Pennock, G. M., and Drury, M. R.: Using a composite flow law to model deformation in the NEEM deep ice core, Greenland – Part 1: The role of grain size and grain size distribution on deformation of the upper 2207 m, The Cryosphere, 14, 2429–2448, https://doi.org/10.5194/tc-14-2429-2020, 2020.

Langway, C. C.: Ice fabrics and the universal stage, SIPRE Tech. Rep., 62, 1958.

Mangeney, A., Califano, F., and Hutter, K.: A numerical study of anisotropic, low Reynolds number, free surface flow for ice sheet modeling, J. Geophys. Res., 102(B10), 22749–22764, https://doi.org/10.1029/97JB01697, 1997.

Matsuda, M., Wakahama, G., and Budd, W. F.: Twinning of ice from Antarctic ice sheet. Observations of a-axis orientation associated with diamond c-axis orientation fabric, Low temperature science (Teion kagaku). Series A Physical sciences, 34, 163-171, 1976.

Matsuda, M., and Wakahama, G.: Crystallographic structure of polycrystalline ice, J. Glaciol., 21, 607-620, https://doi.org/10.3189/S0022143000033724, 1978.

Matsuoka, T., Mae, S., Fukazawa, H., Fujita, S., and Watanabe, O.: Microwave dielectric properties of the ice core from Dome Fuji, Antarctica, Geophys. Res. Lett., 25, 1573–1576, https://doi.org/10.1029/98GL01225, 1998.

Miyamoto, A., Weikusat, I., and Hondoh, T.: Complete determination of ice crystal orientation using Laue X-ray diffraction method. J. Glaciol., 57(201), 103–110, https://doi.org/10.3189/002214311795306754, 2011.

Montagnat, M., Durand, G., and Duval, P.: Recrystallization processes in granular ice, in: Physics of Ice Core Records II, edited by: Hondoh, T., Hokkaido University Press, Sapporo, 81–90, 2009.

Montagnat, M., Buiron, D., Arnaud, L., Broquet, A., Schlitz, P., Jacob, R., and Kipfstuhl, S.: Measurements and numerical simulation of fabric evolution along the Talos Dome ice core, Antarctica, Earth and Planetary Science Letters, 357-358, 168-178, https://doi.org/10.1016/j.epsl.2012.09.025, 2012.

Montagnat, M., Azuma, N., Dahl-Jensen, D., Eichler, J., Fujita, S., Gillet-Chaulet, F., Kipfstuhl, S., Samyn, D., Svensson, A., and Weikusat, I.: Fabric along the NEEM ice core, Greenland, and its comparison with GRIP and NGRIP ice cores, The Cryosphere, 8, 1129-1138, https://doi.org/10.5194/tc-8-1129-2014, 2014.

Montagnat, M., Chauve, T., Barou, F., Tommasi, A., Beausir, B., and Fressengeas, C.: Analysis of Dynamic Recrystallization of Ice from EBSD Orientation Mapping, Front. Earth Sci., 3, 81, https://doi.org/10.3389/feart.2015.00081, 2015.

Montagnat, M., Löwe, H., Calonne, N., Schneebeli, M., Matzl, M., and Jaggi, M.: On the Birth of Structural and Crystallographic Fabric Signals in Polar Snow: A case study from the EastGRIP snowpack, Frontiers in Earth Science, 8, https://doi.org/10.3389/feart.2020.00365, 2020.

Monz, M. E., Hudleston, P. J., Prior, D. J., Michels, Z., Fan, S., Negrini, M., Langhorne, P. J., and Qi, C.: Full crystallographic orientation (c and a axes) of warm, coarse-grained ice in a shear-dominated setting: a case study, Storglaciären, Sweden, The Cryosphere, 15, 303–324, https://doi.org/10.5194/tc-15-303-2021, 2021.

Motoyama, H., Takahashi, A., Tanaka, Y., Shinbori, K., Miyahara, M., Yoshimoto, T., Fujii, Y., Furusaki, A., Azuma, N., and Ozawa, Y.: Deep ice core drilling to a depth of 3035.22 m at Dome Fuji, Antarctica in 2001–07, Ann. Glaciol., 62(85-86), 212–222, https://doi.org/10.1017/aog.2020.84, 2020.

Nakamura, T., and Jones, S.: Softening effect of dissolved hydrogen chloride in ice crystals, Scripta Metallurgica, 4(2), 123–126, https://doi.org/10.1016/0036-9748(70)90176-6, 1970.

Ohno, H., Igarashi, M., and Hondoh, T.: Salt inclusions in polar ice core: Location and chemical form of water soluble impurities, Earth Planet. Sc. Lett., 232, 171–178, https://doi.org/10.1016/j.epsl.2005.01.001, 2005.

Ohno, H., Iizuka, Y., Hori, A., Miyamoto, A., Hirabayashi, M., Miyake, T., Kuramoto, T., Fujita, S., Segawa, T., Uemura, R., Sakurai, T., Suzuki, T., and Motoyama, H.: Physicochemical properties of bottom ice from Dome Fuji, inland East Antarctica, J. Geophys. Res., 121(7), 1230–1250, https://doi.org/10.1002/2015JF003777, 2016.

Oyabu, I., Iizuka, Y., Kawamura, K., Wolff, E., Severi, M., Ohgaito, R., et al., Compositions of dust and sea salts in the Dome C and Dome Fuji ice cores from Last Glacial Maximum to early Holocene based on ice sublimation and single particle measurements. J. Geophys. Res., 125, e2019JD032208. https://doi.org/10.1029/2019JD032208, 2020.

Oyabu, I., Kawamura, K., Buizert, C., Parrenin, F., Orsi, A., Kitamura, K., Aoki, S., and Nakazawa, T.: The Dome Fuji ice core DF2021 chronology (0–207 kyr BP), Quaternary Sci. Rev., 294, 107754, https://doi.org/10.1016/j.quascirev.2022.107754, 2022.

Oyabu, I., Kawamura, K., Fujita, S., Inoue, R., Motoyama, H., Fukui, K., Hirabayashi, M., Hoshina, Y., Kurita, N., Nakazawa, F., Ohno, H., Sugiura, K., Suzuki, T., Tsutaki, S., Abe-Ouchi, A., Niwano, M., Parrenin, F., Saito, F., and Yoshimori, M.: Temporal variations of surface mass balance over the last 5000 years around Dome Fuji, Dronning Maud Land, East Antarctica, Clim. Past, 19, 293–321, https://doi.org/10.5194/cp-19-293-2023, 2023.

Parrenin, F., Fujita, S., Abe-Ouchi, A., Kawamura, K., Masson-Delmotte, V., Motoyama, H., Saito, F., Severi, M., Stenni, B., Uemura, R., and Wolff, E. W.: Climate dependent contrast in surface mass balance in East Antarctica over the past 216 ka, Journal of Glaciology, 1-12, https://doi.org/10.1017/jog.2016.85, 2016, 2016.

Paterson, W. S. B.: Why ice-age ice is sometimes "soft", Cold Reg. Sc. Tech., 20, 75-98, https://doi.org/10.1016/0165-232X(91)90058-O, 1991.

Pattyn, F., Perichon, L., Aschwanden, A., Breuer, B., de Smedt, B., Gagliardini, O., Gudmundsson, G. H., Hindmarsh, R. C. A., Hubbard, A., Johnson, J. V., Kleiner, T., Konovalov, Y., Martin, C., Payne, A. J., Pollard, D., Price, S., Rückamp, M., Saito, F., Souček, O., Sugiyama, S., and Zwinger, T.: Benchmark experiments for higher-order and full-Stokes ice sheet models (ISMIP–HOM), The Cryosphere, 2, 95–108, https://doi.org/10.5194/tc-2-95-2008, 2008.

Pattyn, F.: Antarctic subglacial conditions inferred from a hybrid ice sheet/ice stream model, Earth Planet. Sc. Lett., 295(3–4), 451–461, https://doi.org/10.1016/j.epsl.2010.04.025, 2010.

Petrenko, V. F., and Whitworth, R. W.: Physics of Ice, Oxford University Press, Oxford, 1999.

Pimienta, P., Duval, P., and Lipenkov, V. Y.: Mechanical Behavior of Ice Along the 2040-m Vostok Core, Antarctica, Ann. Glaciol., 10, 137-140, https://doi.org/10.3189/S0260305500004316, 1988.

Poirier J.-P. 1985. Creep of Crystals. Cambridge Earth Science Series. Xiv, Cambridge University Press. ISBN 0 521 26177, Geological Magazine, 122, 579-580, https://doi.org/10.1017/S0016756800035664, 1985.

Qi, C., Prior, D. J., Craw, L., Fan, S., Llorens, M. G., Griera, A., Negrini, M., Bons, P. D., and Goldsby, D. L.: Crystallographic preferred orientations of ice deformed in direct-shear experiments at low temperatures, The Cryosphere, 13, 351-371, https://doi.org/10.5194/tc-13-351-2019, 2019.

Richards, D. H., Pegler, S. S., Piazolo, S., Stoll, N., & Weikusat, I.: Bridging the gap between experimental and natural fabrics: Modeling ice stream fabric evolution and its comparison with ice-core data. Journal of Geophysical Research: Solid Earth, 128, e2023JB027245. https://doi.org/10.1029/2023JB027245, 2023.

Russell-Head, D. S. and Budd, W. F.: Ice-sheet flow properties derived from bore-hole shear measurements combined with ice-core studies, J. Glaciol., 24, 117-130, https://doi.org/10.3189/S0022143000014684, 1979.

Saruya, T., Fujita, S., and Inoue, R.: Dielectric anisotropy as indicator of crystal orientation fabric in Dome Fuji ice core: method and initial results, J. Glaciol., 68(267), 65–76, https://doi.org/10.1017/jog.2021.73, 2022a.

Saruya, T., Fujita, S., Iizuka, Y., Miyamoto, A., Ohno, H., Hori, A., Shigeyama, W., Hirabayashi, M., and Goto-Azuma, K.: Development of crystal orientation fabric in the Dome Fuji ice core in East Antarctica: implications for the deformation regime in ice sheets, The Cryosphere 16(7), 2985–3003, https://doi.org/10.5194/tc-16-2985-2022, 2022b.

Shoji, H., and Higashi, A.: A deformation mechanism map of ice, J. Glaciol., 85(21), 419–427, https://doi.org/10.3189/S002214300003358X, 1978.

Shoji, H. and Langway Jr., C. C.: Mechanical Properties of Fresh Ice Core from Dye 3, Greenland. In: Greenland Ice Core: Geophysics, Geochemistry, and the Environment, https://doi.org/10.1029/GM033p0039, 1985.

Steinbach, F., Kuiper, E.-J. N., Eichler, J., Bons, P. D., Drury, M. R., Griera, A., Pennock, G. M., and Weikusat, I.: The Relevance of Grain Dissection for Grain Size Reduction in Polar Ice: Insights from Numerical Models and Ice Core Microstructure Analysis, Front. Earth Sci., 5, https://doi.org/10.3389/feart.2017.00066, 2017.

Stoll, N., Eichler, J., Hörhold, M., Erhardt, T., Jensen, C., and Weikusat, I.: Microstructure, micro-inclusions, and mineralogy along the EGRIP ice core – Part 1: Localisation of inclusions and deformation patterns, The Cryosphere, 15, 5717–5737, https://doi.org/10.5194/tc- 15-5717-2021, 2021a.

Stoll, N., Eichler, J., Hörhold, M., Shigeyama, W., and Weikusat, I.: A Review of the Microstructural Location of Impurities in Polar Ice and Their Impacts on Deformation, Front. Earth Sci., 8, 615613, https://doi.org/10.3389/feart.2020.615613, 2021b.

Stoll, N., Hörhold, M., Erhardt, T., Eichler, J., Jensen, C., and Weikusat, I.: Microstructure, micro-inclusions, and mineralogy along the EGRIP (East Greenland Ice Core Project) ice core – Part 2: Implications for palaeo-mineralogy, The Cryosphere, 16, 667–688, https://doi.org/10.5194/tc-16-667-2022, 2022.

~~Thomas, R. E., Negrini, M., Prior, D. J., Mulvaney, R., Still, H., Bowman, M. H., Craw, L., Fan, S., Hubbard, B., Hulbe, C., Kim, D., and Lutz, F.: Microstructure and Crystallographic Preferred Orientations of an Azimuthally Oriented Ice Core from a Lateral Shear Margin: Priestley Glacier, Antarctica, 9, https://doi.org/10.3389/feart.2021.702213, 2021.~~

Thorsteinsson, T., Kipfstuhl, J. and Miller, H.: Textures and fabrics in the GRIP ice core, J. Geophys. Res., 102(C12), 26583–26599, https://doi.org/10.1029/97JC00161, 1997.

~~Thorsteinsson, T., Waddington, E. D., Taylor, K. C., Alley, R. B., and Blankenship, D. D.: Strain- rate enhancement at Dye 3, Greenland, J. Glaciol., 45, 338-345, https://doi.org/10.3189/002214399793377185, 1999.~~

Tsutaki, S., Fujita, S., Kawamura, K., Abe-Ouchi, A., Fukui, K., Motoyama, H., Hoshina, Y., Nakazawa, F., Obase, T., Ohno, H., Oyabu, I., Saito, F., Sugiura, K., and Suzuki, T.: High-resolution subglacial topography around Dome Fuji, Antarctica, based on ground-based radar surveys conducted over 30 years, The Cryosphere, 16, 2967–2983, https://doi.org/10.5194/tc-16-2967-2022, 2022.

~~Urbini, S., Frezzotti, M., Gandolfi, S., Vincent, C., Scarchilli, C., Vittuari, V., and Fily, M.: Historical behaviour of Dome C and Talos Dome (East Antarctica) as investigated by snow accumulation and ice velocity measurements, Glob. Planet. Change, 60, https://doi.org/10.1016/j.gloplacha.2007.08.002, 2008.~~

~~Wang, Q., Fan, S., Richards, D. H., Worthington, R., Prior, D. J., and Qi, C.: Evolution of crystallographic preferred orientations of ice sheared to high strains by equal-channel angular pressing, EGUsphere [preprint], https://doi.org/10.5194/egusphere-2024-331, 2024.~~

~~Wang, Y., Kipfstuhl, S., Azuma, N., Thorsteinsson, T., and Miller, H.: Ice-fabrics study in the upper 1500 m of the Dome C (East Antarctica) deep ice core, Ann. Glaciol., 37, 97-104, https://doi.org/10.3189/172756403781816031, 2003.~~

Weikusat, I., Kipfstuhl, S., Faria, S. H., Azuma, N., and Miyamoto, A.: Subgrain boundaries and related microstructural features in EDML (Antarctica) deep ice core, J. Glaciol., 55, 461-472, https://doi.org/10.3189/002214309788816614, 2009.

Weikusat, I., Jansen, D., Binder, T., Eichler, J., Faria, S. H., Wilhelms, F., Kipfstuhl, S., Sheldon, S., Miller, H., Dahl-Jensen, D., and Kleiner, T.: Physical analysis of an Antarctic ice core – towards an integration of micro- and macrodynamics of polar ice, Phil. Trans. R. Soc. A, 375, 20150347, http://dx.doi.org/10.1098/rsta.2015.0347, 2017.

~~Wolff, E. W., Fischer, H., van Ommen, T., and Hodell, D. A.: Stratigraphic templates for ice core records of the past 1.5 Myr, Clim. Past, 18, 1563–1577, https://doi.org/10.5194/cp-18-1563-2022, 2022.~~

Yamanouchi, T., Hirasawa, N., Hayashi, M., Takahashi, S., and Kaneto, S.: Meteorological characteristics of Antarctic inland station, Dome Fuji. Mem. Natl Inst. Polar Res., Spec. Issue, 57, 94–104, 2003.

~~Young, D. A., Roberts, J. L., Ritz, C., Frezzotti, M., Quartini, E., Cavitte, M. G. P., Tozer, C. R., Steinhage, D., Urbini, S., Corr, H. F. J., van Ommen, T., and Blankenship, D. D.: High-resolution boundary conditions of an old ice target near Dome C, Antarctica, The Cryosphere, 11, 1897–1911, https://doi.org/10.5194/tc-11-1897-2017, 2017.~~